

# Mineral Chemistry of Two-Mica Granite Rare Metals: Impact of Geophysics on the Distribution of Uranium Mineralization at El Sela Shear Zone, Egypt

Ibrahim Gaafar<sup>1</sup>, Michel Cuney<sup>2</sup>, Ahmed Abdel Gawad<sup>1</sup>

<sup>1</sup>Nuclear Materials Authority, Cairo, Egypt

<sup>2</sup>G2R, Nancy-Université, CNRS, CREGU, Lorraine, France

Email: [ibrahim.gaafar@hotmail.com](mailto:ibrahim.gaafar@hotmail.com)

Received 1 March 2014; revised 3 April 2014; accepted 11 April 2014

Copyright © 2014 by authors and Scientific Research Publishing Inc.

This work is licensed under the Creative Commons Attribution International License (CC BY).

<http://creativecommons.org/licenses/by/4.0/>



Open Access

## Abstract

The present work aims at identifying Nb-Ta-, Zr-Hf-, REE-, Th-U-bearing two-mica granite from geological, geophysical cross-sections and mineral chemistry studies from three boreholes at G. El Sela shear zone. Microscopically, the three boreholes are composed mainly of two-mica granite. They are composed of K-feldspar, plagioclase, quartz, biotite and muscovite. Accessories are pyrite, zircon, fluorite, rutile, monazite with Th-U-mineralization identified by scanning electron microscope (SEM) and electron probe-microanalyses (EPMA). Chlorite, muscovite, sericite, kaolinite are secondary minerals. Geochemically, two-mica granite boreholes are A-type granites and peraluminous characteristics. They are enriched in large ion lithophile elements (LILE; Ba, Rb and Sr), high field strength elements (Y, Zr and Nb), and LREE but depleted in HREE with negative Eu anomaly. U-enrichment associated with chloritization, muscovitization, albitization, sericitization, kaolinization and argillization results from convective hydrothermal circulation of fluids through brittle structures along the ENE-WSW main shear zone. The ratios Nb/Ta (7.7 - 17.7) and Zr/Hf (16.9 - 26.4) are relatively enriched in the lighter isovalents Ta and Hf. The accessory minerals observed in the two-mica granites are represented by metallic sulfides (pyrite, arsenopyrite, chalcopyrite, galena and sphalerite), Nb-rutile, Hf-zircon, fluorite, monazite, columbite, betafite, thorite, phosphothorite, uranothorite, brannerite, uraninite, coffinite and pitchblende at G. El Sela shear zone. Uraninite with a low Th content indicates a hydrothermal origin of U-mineralization, Thorite, uranothorite, monazite and zircon is the main uranium bearing minerals of magmatic origin within the enclosing granite. The primary U-mineralization has been observed in two boreholes. In order to illustrate the geophysical signature of El Sela U-mineralization, the radiometric, magnetic, and VLF-EM data as well as radon concentration are included. The magnetic, electrical conductivity and radiometric profiles were produced from detailed ground surveys. The shear zone is cha-

characterized by relatively weak levels for both K and eTh, but very high eU anomalies (<3500 ppm). Therefore, the Sela shear zone acts as a good trap for U-mineralization. The Sela Shear zone coincides with positive conductivity anomalies, which are the most prominent features on the respective profiles. The magnetic field over the Sela shear zone is also conspicuous by the sharp contrast which makes with the strong negative signatures of the altered microgranite. The radon distribution map showed the presence of seven high anomalies that are mostly controlled by the structures due to the easy movement of radon through them.

## Keywords

Boreholes, Shear Zone, Radon, Spectrometric, Magnetic, Conductivity

## 1. Introduction

Uranium ore is the indispensable raw material for nuclear fuel preparation and is currently heavily prospected. Unlike the majority of metals, the metallogeny of uranium is specifically characterized by an extreme diversity of deposits that are directly related to the various conditions under which U deposits formed in geological environments [1]. More than 1500 uranium deposits are identified in the UDEPO data base of the AIEA ([http://www.iaea.org/OurWork/ST/NE/NEFW/Technical\\_Areas/NFC/infcis-UDEPO.html](http://www.iaea.org/OurWork/ST/NE/NEFW/Technical_Areas/NFC/infcis-UDEPO.html)) and 16 major deposit types are distinguished by the International Atomic Energy Agency [2].

Generally, granitic rocks are one of the most favourable host rocks for U-mineralization in many parts of the world. Genetically, the economic uranium deposits associated with granites are mostly located in anatectic melts or in strongly peraluminous two-mica granites [3]-[5]. In general, the granites are rich in incompatible elements (Rb, Nb, Sn, Th, and U) [6] [7]. The genetic relationship between granite intrusions and associated U-mineralization has been discussed for a long time. Background uranium concentrations at the scale of the granite plutons crystallize at the magmatic to late magmatic stage as accessory minerals (zircon, monazite, allanite, uranorthite, uraninite...). They represent the primary source of uranium for many deposits and their enrichment rarely reaches economic grades except in some highly fractionated peralkaline granites or anatectic pegmatoids [8]. The formation of an economic uranium concentration generally requires the remobilization of the uranium from these primary sources followed by deposition in tectonic structures with higher grades.

Most Egyptian uranium occurrences in granite rocks of G. Um Ara [9] [10], G. Gattar [11] G. Missikat [12] and G. Erediya [13] [14] are associated with metaluminous to slightly peraluminous granite. Uranium mineralization in these granites belongs to the vein-type except G. Gattar and G. Um Ara, where U-mineralization belongs to the fracture-filling type. The marginal parts of all these granitic intrusions are generally more radioactive than their central parts in relation with the development of different types of alteration, which include silicification, episyenitization, albitization, fluoritization, ferruginization, sericitization, chloritization, kaolinitization and illitization.

El Sela two-mica uraniferous peraluminous granite [15]-[18] is located in the south-eastern part of Egypt between latitudes 22° 16'26" - 22° 18'38"N and longitudes 36° 13'33" - 36° 16'26"E.

## 2. Geologic Setting

El Sela granitic pluton is composed of two-mica (muscovite-biotite) granite intrusions trending ENE-WSW (Figure 1). It is jointed in different directions, and defines low to moderate reliefs. This granite is injected by microgranite, dolerite and bostonite dikes, and quartz and jasperoid veins. They are mostly injected along ENE-WSW and/or NNW-SSE to N-S directions which represent the most important tectonic trends for U anomalies in the study area. Pegmatite pockets are found as irregular bodies in two-mica granite. They are very coarse grained, buff to reddish pink colors, highly sheared and composed of K-feldspar, quartz, plagioclase, biotite with muscovite. They show slightly higher total radioactivity than two-mica granite.

A microgranite dike hosts the most radioactive anomalies in the study area. It is injected into the two-mica granite along an ENE-WSW shear zone with dip of about 75 to south. It is whitish pink, pale pink, reddish pink to pale grey colors and is 3 to 20 m thick.

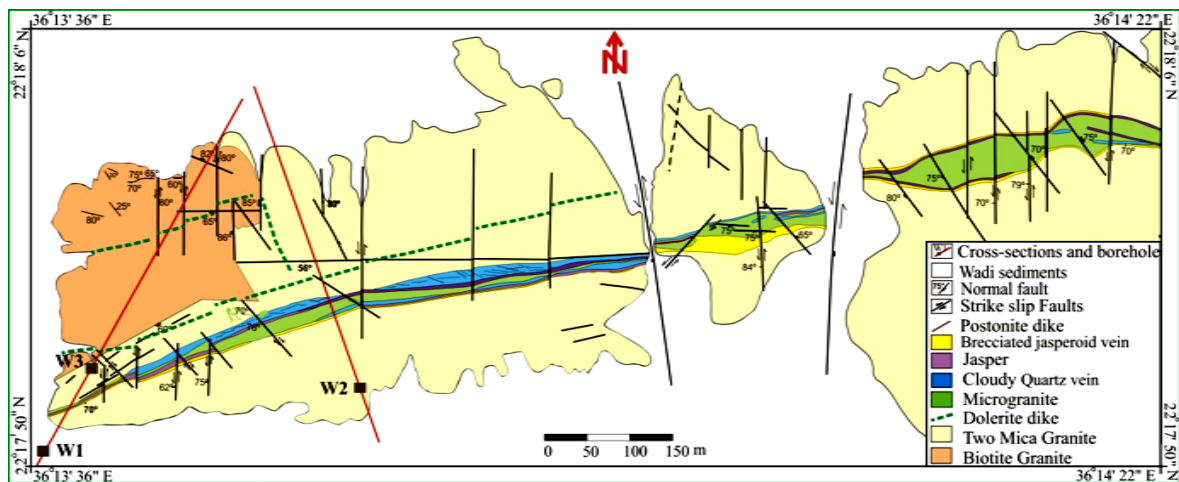


**Figure 1.** Detailed geological map of the main shear zone at G. El Sela area, south E D, Egypt (after [16]).

It is also essentially composed of quartz, K-feldspar, plagioclase, biotite and muscovite. It is enriched with mineralized with uranophane and pyrite cubes. Ferrugination, silicification, albitization, episyenitization, fluoritization and illitization are different alterations mainly occurring with the ENE-WSW shear zone. Some of these alterations are possibly related to U remobilization, but probably not all. To be discussed in detail later.

Dolerite dikes are greyish green to dark grey colors, fine- to medium-grained and range in thickness from 0.5 to 6 m. They are injected into the two-mica granite along ENE-WSW, NNW-SSE and N-S directions with dip of about 75° to south. They are mainly composed of plagioclase, olivine and pyroxene. Accessories are apatite and opaque minerals while chlorite, sericite and calcite are alteration minerals. The dolerites have higher U-contents which may reach up to 3500 ppm eU and 75 ppm eTh. They are highly altered to clay minerals and cavities are filled with pyrite cubes and/or secondary uranium minerals (uranophane and autunite). Many open cuts have been made to recognize the importance of the U mineralization within the microgranite and dolerite dikes. Many semi-industrial technological procedures for the leaching and recovery of the U incorporated within these mineralized dikes have been performed.

Along the main ENE-WSW shear zone three generations of quartz veins with different colors have been identified. The milky quartz vein occurs at the shear margins, is the oldest one, highly brecciated, barren, and range in thickness from 1 to 4 m. The milky quartz vein is crosscut by two younger generations of quartz with obvious displacement. Red and grey to black jasper veins are commonly parallel to the shear zone and the older milky quartz vein and are mineralized. They are strongly jointed, fragmented, brecciated and are 0.5 to 1 m thick, contain macroscopically visible pyrite and uranophane. Within the ENE-WSW shear zone, the quartz veins brecciate the microgranite and dolerite dikes. Some other quartz veins are trending NNW-SSE and N-S. Bostonite dikes invade two-mica granite along N-S and NNE-SSW structures. They are usually fine-grained, pale brown to deep red colors, fractured, jointed, sheeted, and range in thickness from 0.5 to 2 m. They are essentially composed of K-feldspar, plagioclase, little quartz and iron oxides set in a finely crystalline groundmass of K-feldspar micro-lites. They have U-contents from 4.1 to 25.4 ppm eU.

The Sela shear zone is clearly evidenced from its rugged topography by a sharp increase in the eU values as well as from a marked decrease of the K and eTh values. These characteristics result from multiple magmatic, tectonic and hydrothermal activities, confined to a wide elongated domain of average 20 m in width and 1.5 km [19]. The relatively narrow and elongated shape of the Sela shear zone magnetic anomaly is consistent with the steep dip of the magnetized shear zone. This should be related to the nature of the intruding dykes rather than from the mineralization. The prominence of this anomaly can be attributed to the strong contrast between the magnetic susceptibilities of the Sela shear zone, and the surrounding granitic rocks. The northern contact between the granitic body and the wadi sediments is characterized by an elongated low magnetic gradient, trending in the ENE-WSW direction, parallel to the main shear zone indicate the presence of a major basement fault [20]. The main zone of strong conductivity has been separated into parts of high amplitudes, resulting in an obvious exploration target. This zone is found on a broader discrete area, extending over a distance of about 1500 m and subjected to northeast displacements, due to a parallel system of NNW left-lateral strike-slip faults [21].

### 3. Methodology

Solid state nuclear track detectors (SSNTDs) have been recognized by IAEA as a standard method for estimation of radon, thoron and their daughter products in the environment. The detectors that are commonly used in environmental monitoring are generally made from cellulose nitrate (LR-115) and polycarbonates (CR-39). These Track Etch cups are placed in shallow holes (30 - 50 cm) and left undisturbed for one month to accumulate the tracks produced by the radon soil emanations. Track Etch detectors are responsive to the alpha radiation from radon (Rn-222) which originates from radium (Ra-226) in the uranium (U-238) decay chain as well as to thoron (Rn-220) which originates from radium (Ra-224) in the thorium (Th-232) decay chain. The track density is converted to radon concentration in the environment. The radon concentration was calculated through the following equation [22]:  $C = D/k \cdot t$ . Where;  $C$  is the radon concentration (Bq/m<sup>3</sup>),  $D$  is the track density (track/cm<sup>2</sup>),  $k$  is the calibration factor and  $t$  is the exposure time (d).

Track Etch detectors are responsive to the alpha radiation from radon (Rn-222) which originates from radium (Ra-226) in the uranium (U-238) decay chain as well as to Thoron (Rn-220) which originates from radium (Ra-224) in the thorium (Th-232) decay chain. Thus, if significant amounts of thorium are present in the area that is being explored, it can produce an unwanted thorium related signal when looking for uranium. In the present work the cups which have been used have been produced by ALGADE. They use a solid-state nuclear track detector type Kodak LR115R films. They have a water tight polyethylene membrane to avoid water entrances and which is used also as a thoron filter. This membrane decrease de rate of passage of throne into the cup (because of its short half-life) bu allows radon to pass into the cup. The radon concentration in the cup is not reduced significantly by this kind of filter.

The ground geophysical studies get information about the subsurface configuration of the shear structures controlling uranium mineralized zones. In studied area, Track Etch survey (60 cups) for radon gas were placed in shallow bore holes (30 - 65 cm deep) and undisturbed left for 1 - 1.5 month to accumulate the reading produced by the varying radon soil activities.

The ground gamma-ray spectrometric measurements were conducted using a Geophysica Brno GS-256 spectrometer having a 0.35 L sodium iodide (NaI) thallium activated detector. All the ground magnetic and VLF measurements were collected using the Scintrex proton magnetometer and ENVI-VLF. The data were generally recorded of 20 m spacing interval along each of the two studied profiles.

Twenty samples were selected from the host rocks two-mica granite of three drill cores from the El Sela shear zone. Minerals were investigated in thin polished and thick double-polished sections using optical microscope and scanning electron microscope (Hitachi S-4800, SCMEM, Henri Poincaré University, France). Minerals were analysed by electron microprobe (CAMECA SX 100, SCMEM, Henri Poincaré University, France) at 10 nA and at 20 kV, counting time 10 s for peak and 5 s for background. Natural albite, orthoclase, wollastonite, hematite, olivine and monazite were used as standards for Al (K $\alpha$ ), Si (K $\alpha$ ), Ca (K $\alpha$ ), Fe (K $\alpha$ ), Mg (K $\alpha$ ) and Yb (L $\alpha$ ), respectively; synthetic V, ZrO<sub>2</sub>, PbCrO<sub>4</sub>, UO<sub>2</sub>, MnTiO<sub>3</sub>, ThO<sub>2</sub>, MnTiO<sub>3</sub>, YPO<sub>4</sub>, CePO<sub>4</sub>, NdPO<sub>4</sub>, SmPO<sub>4</sub>, DyRu<sub>2</sub>Ge<sub>2</sub>, EuRu<sub>2</sub>Ge<sub>2</sub>, GdTlGe and ErNi<sub>2</sub>Si<sub>2</sub> were used as standards for V (K $\alpha$ ), Zr (L $\alpha$ ), Pb (M $\alpha$ ), U (M $\beta$ ), Ti (K $\alpha$ ), Th (M $\alpha$ ), Mn (K $\alpha$ ), Y (L $\alpha$ ), Ce (L $\alpha$ ), Nd (L $\alpha$ ), Sm (L $\alpha$ ), Dy (L $\alpha$ ), Eu (L $\alpha$ ), Gd (L $\alpha$ ), Er (L $\alpha$ ), respectively. After agate mortar crushing, the rocks were analysed by ICP-AES and ICP-MS (SARM, CRPG, Nancy, France) for 11 major and 44 trace elements.

### 4. Petrography of Boreholes

The three boreholes are composed mainly of two-mica granite. It is whitish to pale pink, buff, reddish brown, medium- to coarse-grained, highly fractured and jointed. Microscopically, it is composed essentially of K-feldspar, quartz, plagioclase, biotite and muscovite. Monazite, pyrite, Zircon, galena, sphalerite, Nb-rutile, columbite, titanite, apatite, fluorite and uraninite are accessories, while sericite, chlorite, muscovite, epidote and kaolinite are alteration minerals.

K-feldspar is represented by orthoclase micropertthite. It occurs as subhedral to anhedral prismatic crystals showing simple twinning and compressed patchy, string and flame perthitic intergrowths (Figure 2(a)). It encloses fine plagioclase, quartz, biotite inclusions and can be highly altered into kaolinite (Figure 2(b)). Quartz occurs as interstitial subhedral to anhedral crystals. It shows wavy and undulose extinction. Some small anhedral crystals poikilitically occur in perthite, plagioclase and biotite. Plagioclase of albite and oligoclase composition (An<sub>9-15</sub>) occurs as subhedral to euhedral tabular crystals. Biotite occurs as subhedral flakes, which are commonly

altered to ferrichlorite (pennite) and/or muscovite along the crystal margins and cleavage planes (**Figure 2(c)**). It is corroded by K-feldspar and quartz its margins. Muscovite occurs as minor irregular fine or medium grained flakes of seldom primary and generally secondary origin (**Figure 2(d)**). The overgrowths on the primary muscovite grains tend to replace adjacent K-feldspars and quartz grains. The secondary muscovite is formed after biotite and contained elongated iron-titanium inclusions along its cleavage.

Zircons occur as metamict, zoned, mostly euhedral crystals with prismatic a shape and bipyramidal terminations, associated with quartz, perthite, plagioclase and opaques (**Figure 2(e)**). Nb-rutile occurs as crystal of pale brown color enclosed in feldspars (**Figure 2(f)**). Opaque minerals occur as cubic crystals, small irregular aggregates or scattered grains as well as tiny inclusions in biotite and quartz. Uraninite filled micro-fractures in kaolintized and sericitized feldspars and generally surrounded by pyrite cubes (**Figure 2(g)**, **Figure 2(h)**).

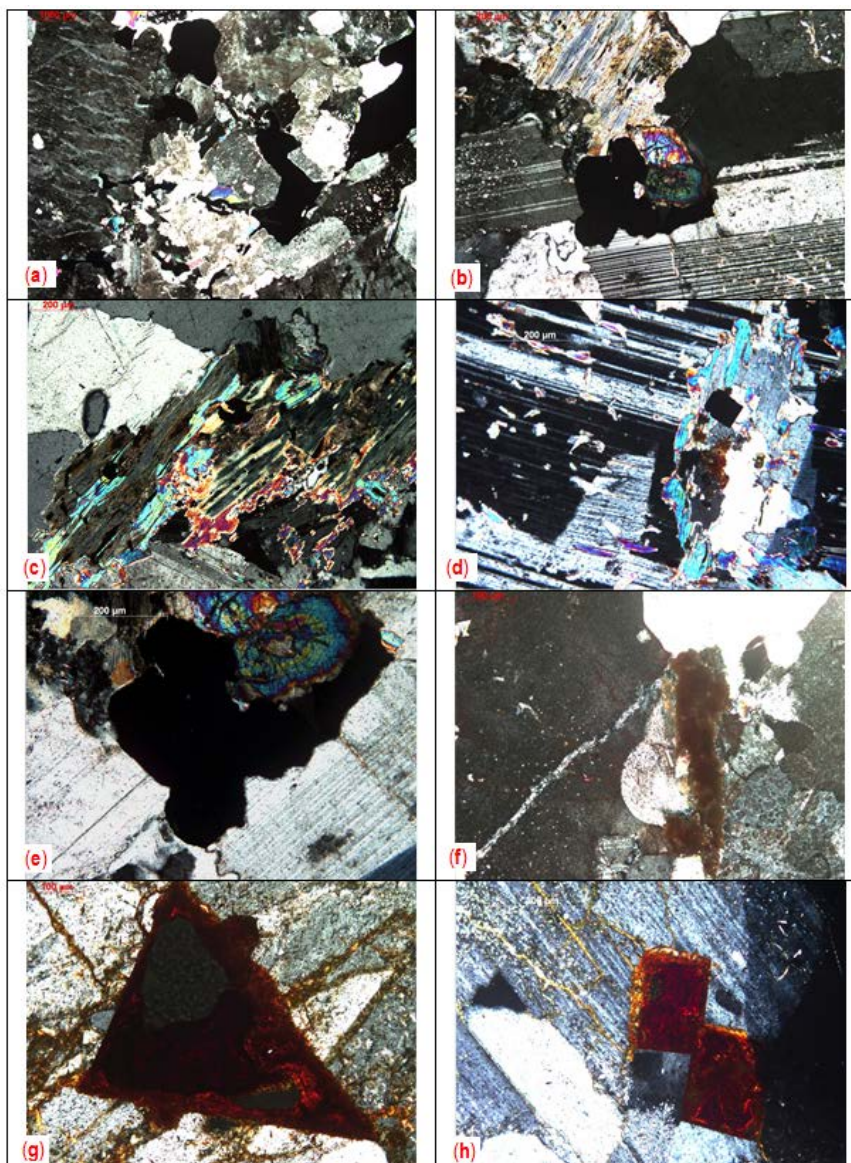


**Figure 2.** Photomicrographs for El Sela shear zone granites: (a) String and patchy perthites. (b) Feldspars altered to kaolinite and sericite with opaques enclosed zircon. (c) Biotite crystals highly altered to ferrichlorite (pennite) and muscovite. (d) Muscovite flake corroding adjacent plagioclase, and poikilitically encloses opaques and quartz. (e) Zircon crystals show zonation enclosed in pyrite (opaque). (f) Nb-rutile has elongated shape. (g), (h) Uraninite filled microfractures with pyrite in kaolinized and sericitized feldspars.

## 5. Geochemistry

The geochemical data have been used to determine the characteristics of granites enclosing the Sela shear zone and their uranium fertility. The uranium fertility of the granites depends essentially on the level of their U background concentration and the leache ability of the uranium bearing accessory minerals. Peraluminous, high-K and low Na and Ca contents and presence of two-mica are also good indicators of the U-fertility of granite rocks. Under certain conditions of alteration, the high-calc-alkaline (HKCA) granite can form uranium ore but generally with lesser tonnage than the peraluminous leucogranites [8].

### 5.1. Major Elements

El Sela two-mica granites have high SiO<sub>2</sub>, Al<sub>2</sub>O<sub>3</sub>, Na<sub>2</sub>O and K<sub>2</sub>O contents with the following average contents 76.5 wt.%, 12.95 wt.%, 3.9 wt.% and 4.3 wt.%, respectively. They are also poor in Fe<sub>2</sub>O<sub>3</sub>, CaO, MnO and MgO with average concentrations of 0.73 wt.%, 0.53 wt.%, 0.04 wt.% and 0.17 wt.%, respectively **Table 1**.

**Table 1.** Chemical analyses of the samples from the bore holes of the El Sela two-mica granite.

| S. No.                         | W1-1  | W1-2  | W1-3  | W1-4 | W1-5 | W1-6 | W1-7 | W1-8 | W2-1 | W2-2 | W2-3 | W2-4 | W2-5 | W2-6 | W2-7 | W2-8 | W2-9 | W3-1 | W3-2 | W3-3 |
|--------------------------------|-------|-------|-------|------|------|------|------|------|------|------|------|------|------|------|------|------|------|------|------|------|
| depth m.                       | 20    | 24    | 35    | 53   | 55   | 59   | 62   | 63   | 1    | 4    | 10   | 17   | 26   | 35   | 37   | 42   | 44   | 12   | 30   | 43   |
| Major oxides (wt.%)            |       |       |       |      |      |      |      |      |      |      |      |      |      |      |      |      |      |      |      |      |
| SiO <sub>2</sub>               | 76.2  | 76.3  | 77.7  | 74.6 | 76.9 | 76.2 | 76.9 | 76   | 77.4 | 76.8 | 76.7 | 76.8 | 78   | 77.5 | 76.8 | 74.8 | 76.8 | 75.5 | 77   | 74.7 |
| TiO <sub>2</sub>               | 0.13  | 0.13  | 0.13  | 0.10 | 0.12 | 0.10 | 0.09 | 0.13 | 0.10 | 0.10 | 0.10 | 0.14 | 0.10 | 0.14 | 0.12 | 0.16 | 0.14 | 0.13 | 0.13 | 0.09 |
| Al <sub>2</sub> O <sub>3</sub> | 13.3  | 13.3  | 12.5  | 12.6 | 12.8 | 13.7 | 12.7 | 13   | 12.9 | 13.3 | 13.2 | 13   | 12.6 | 12.3 | 13.1 | 13.1 | 12.8 | 12.7 | 12.5 | 13.7 |
| Fe <sub>2</sub> O <sub>3</sub> | 0.7   | 0.9   | 0.9   | 1.2  | 0.5  | 0.6  | 0.9  | 0.9  | 0.6  | 0.5  | 0.6  | 0.9  | 0.7  | 0.8  | 0.7  | 0.6  | 0.6  | 0.8  | 0.7  | 0.5  |
| MnO                            | 0.05  | 0.06  | 0.04  | 0.10 | 0.02 | 0.03 | 0.08 | 0.06 | 0.01 | 0.01 | 0.01 | 0.01 | 0.01 | 0.01 | 0.03 | 0.02 | 0.03 | 0.09 | 0.08 | 0.06 |
| MgO                            | 0.12  | 0.22  | 0.15  | 0.12 | 0.07 | 0.11 | 0.12 | 0.16 | 0.10 | 0.09 | 0.10 | 0.19 | 0.23 | 0.25 | 0.17 | 0.35 | 0.38 | 0.20 | 0.16 | 0.12 |
| CaO                            | 0.5   | 0.3   | 0.2   | 0.9  | 0.2  | 0.4  | 0.7  | 0.8  | 0.4  | 0.4  | 0.4  | 0.5  | 0.3  | 0.3  | 0.4  | 1    | 0.4  | 1.1  | 0.7  | 0.7  |
| Na <sub>2</sub> O              | 4.4   | 3.8   | 4     | 4.1  | 4.1  | 4.5  | 4.2  | 4.3  | 4    | 4.4  | 4.1  | 4    | 3.2  | 3    | 4.1  | 2.8  | 2.6  | 4.1  | 4.3  | 4.3  |
| K <sub>2</sub> O               | 4.1   | 4.2   | 3.7   | 4.2  | 4.2  | 4.5  | 4.3  | 4.3  | 4.6  | 4.5  | 4.8  | 4.3  | 4    | 4.2  | 4.4  | 4.2  | 4.4  | 4    | 3.8  | 5    |
| P <sub>2</sub> O <sub>5</sub>  | 0.1   | 0.1   | 0.1   | 0    | 0    | 0.1  | 0.1  | 0.1  | 0.1  | 0.1  | 0.1  | 0.2  | 0.1  | 0.1  | 0.1  | 0.2  | 0.2  | 0.1  | 0.1  | 0.1  |
| IL                             | 0.8   | 1.5   | 0.9   | 1.6  | 1    | 1    | 1.1  | 1.1  | 0.7  | 0.7  | 0.7  | 1    | 1.9  | 2    | 1.1  | 3.1  | 2.8  | 1.4  | 1.2  | 0.9  |
| Total                          | 100   | 101   | 100   | 100  | 100  | 101  | 101  | 101  | 101  | 101  | 101  | 101  | 101  | 101  | 101  | 100  | 101  | 100  | 101  | 100  |
| Trace elements (ppm)           |       |       |       |      |      |      |      |      |      |      |      |      |      |      |      |      |      |      |      |      |
| Be                             | 5.4   | 4.4   | 4.9   | 8.4  | 3.2  | 5.4  | 7.4  | 7.6  | 3.1  | 3.5  | 2.8  | 4.2  | 2.9  | 4.1  | 5.2  | 3.4  | 3.5  | 7.8  | 8.5  | 8.7  |
| Sc                             | 4.9   | 5.1   | 5.2   | 6.8  | 3.9  | 5.1  | 6.7  | 7.7  | 3.4  | 2.6  | 2.6  | 4.1  | 2.3  | 3.8  | 4.1  | 3.8  | 3.6  | 8.4  | 7.7  | 6.2  |
| Ti                             | 1.6   | 1.6   | 1.6   | 1.2  | 1.5  | 1.3  | 1.2  | 1.6  | 1.3  | 1.2  | 1.3  | 1.8  | 1.2  | 1.7  | 1.5  | 2    | 1.7  | 1.6  | 1.6  | 1.2  |
| V                              | 9.7   | 8.7   | 9.1   | 5.8  | 6.3  | 5.6  | 4.4  | 5.8  | 5.2  | 5.1  | 3.5  | 8.2  | 3.6  | 7.9  | 6.6  | 8.2  | 6.8  | 8.2  | 6.7  | 5.5  |
| Cr                             | 62.2  | 132   | 95    | 100  | 62.7 | 89   | 70.3 | 78.9 | 80.2 | 50.3 | 62.7 | 93   | 93   | 88   | 92   | 78.2 | 83   | 77.8 | 95   | 69   |
| Mn                             | 0.8   | 0.8   | 0.6   | 1.4  | 0.2  | 0.4  | 1.1  | 0.9  | 0.1  | 0.1  | 0.1  | 0.2  | 0.2  | 0.1  | 0.4  | 0.3  | 0.4  | 1.3  | 1.1  | 0.8  |
| Co                             | 0.8   | 1.5   | 1.4   | 1.8  | 0.7  | 0.9  | 1.1  | 1.1  | 0.6  | 0.8  | 0.7  | 1.1  | 0.9  | 0.8  | 1    | 0.9  | 0.9  | 1    | 0.9  | 0.7  |
| Zn                             | 35.2  | 39.5  | 30    | 57.9 | 24.7 | 33.9 | 45.9 | 78   | 39.7 | 33   | 29.4 | 59   | 38.9 | 27.3 | 48.8 | 62.1 | 36.7 | 51.2 | 57.3 | 43.2 |
| Ga                             | 24    | 24    | 23    | 26   | 21   | 25   | 25   | 27   | 21   | 21   | 22   | 23   | 20   | 21   | 25   | 23   | 23   | 25   | 26   | 30   |
| Ge                             | 1.5   | 1.4   | 1.7   | 2.2  | 1.3  | 1.8  | 2.2  | 2.2  | 1.3  | 1.4  | 1.4  | 1.5  | 1.3  | 1.5  | 1.9  | 1.4  | 1.3  | 2    | 2.2  | 3    |
| Rb                             | 248.8 | 275.5 | 244.6 | 427  | 211  | 280  | 412  | 394  | 195  | 184  | 206  | 188  | 174  | 204  | 267  | 196  | 198  | 364  | 357  | 464  |

## Continued

|                       |      |      |      |      |      |      |      |      |      |      |      |      |      |      |      |      |      |      |      |      |
|-----------------------|------|------|------|------|------|------|------|------|------|------|------|------|------|------|------|------|------|------|------|------|
| Sr                    | 151  | 121  | 107  | 79   | 101  | 72   | 72   | 100  | 55   | 103  | 47   | 99   | 62   | 110  | 89   | 116  | 96   | 91   | 110  | 87   |
| Y                     | 7.2  | 6.7  | 6.9  | 4.8  | 5.1  | 4.3  | 4.9  | 5.3  | 11.3 | 4.2  | 3    | 6.4  | 3.4  | 5.9  | 5.8  | 19.9 | 5.4  | 5.4  | 7.2  | 5.7  |
| Zr                    | 90.4 | 88.2 | 85.6 | 66.9 | 80.9 | 69.5 | 66.2 | 92.5 | 62.8 | 62.2 | 53.7 | 79.3 | 68.4 | 82   | 73   | 89   | 80   | 88   | 97   | 61   |
| Nb                    | 13.7 | 13.3 | 14.8 | 16.4 | 9.5  | 13.2 | 16   | 22.9 | 7.2  | 5.7  | 5.3  | 6.9  | 5.3  | 8.9  | 14.5 | 9.3  | 7.1  | 22.3 | 21.1 | 31.4 |
| Mo                    | 0.8  | 2.7  | 1.3  | 2.6  | 0.9  | 2    | 2.9  | 3.4  | 1.2  | 0.8  | 1    | 1.6  | 1.3  | 1.2  | 1.3  | 1.1  | 1.1  | 3.7  | 5.3  | 1.3  |
| Sn                    | 2.1  | 2.6  | 2.2  | 5.8  | 1.5  | 1.6  | 2.3  | 2.5  | 1.1  | 0.9  | 1.1  | 1.5  | 0.7  | 1.4  | 1.5  | 1.7  | 1.7  | 2.8  | 2.7  | 2.1  |
| Cs                    | 5.9  | 6.3  | 4.6  | 11.5 | 4    | 6.9  | 10.2 | 10.9 | 4.5  | 5.2  | 4.4  | 7.5  | 2.9  | 3.8  | 6.6  | 4.8  | 5    | 10.2 | 10.1 | 11.7 |
| Ba                    | 351  | 296  | 222  | 137  | 263  | 155  | 132  | 173  | 147  | 261  | 83   | 198  | 94   | 179  | 167  | 204  | 213  | 154  | 168  | 167  |
| Hf                    | 4.2  | 3.9  | 4.4  | 3.5  | 3.3  | 3.3  | 3.6  | 4.7  | 2.7  | 2.8  | 2.2  | 3    | 2.8  | 3.5  | 3.3  | 3.5  | 3.4  | 4.4  | 4.7  | 3.6  |
| Ta                    | 1.7  | 1.6  | 1.8  | 1.8  | 1.1  | 1.5  | 1.8  | 2.2  | 0.8  | 0.5  | 0.5  | 0.9  | 0.3  | 0.9  | 1.7  | 1    | 0.7  | 2.1  | 2.2  | 3.9  |
| W                     | 3.7  | 12.9 | 10.6 | 6.4  | 4.3  | 5.7  | 4.5  | 5.1  | 5.5  | 3.3  | 4.6  | 6.8  | 6.2  | 6.2  | 6    | 5.9  | 5.7  | 5.4  | 6.8  | 4.5  |
| Pb                    | 27.4 | 23.9 | 30.1 | 36.3 | 18.3 | 21.8 | 43   | 32.4 | 17.9 | 16.6 | 14.9 | 19   | 20.5 | 13.8 | 25.7 | 22   | 21.8 | 34.8 | 67   | 50   |
| Th                    | 18.3 | 18.1 | 16.3 | 22.5 | 17.3 | 19.9 | 23.2 | 29   | 21   | 13   | 23   | 17   | 24   | 18   | 18   | 20   | 16   | 28   | 29   | 19.6 |
| U                     | 6    | 7.8  | 8.1  | 15   | 4.1  | 9.5  | 18   | 33   | 5.8  | 3.2  | 3.4  | 4.7  | 3.9  | 4.4  | 9.1  | 7.5  | 3.9  | 15   | 23   | 25   |
| REE (ppm)             |      |      |      |      |      |      |      |      |      |      |      |      |      |      |      |      |      |      |      |      |
| La                    | 14.7 | 15.1 | 12.9 | 13   | 12.5 | 13.4 | 14.8 | 21   | 17   | 13.4 | 17.4 | 16.3 | 12.4 | 19.8 | 15.7 | 22.9 | 17.8 | 18.5 | 20.1 | 14   |
| Ce                    | 29.2 | 29.3 | 27.8 | 18.6 | 20.9 | 18.3 | 22   | 29.5 | 27.7 | 21.8 | 25.2 | 25.5 | 20.3 | 26.6 | 25.1 | 39.5 | 30.4 | 26.6 | 27.9 | 20   |
| Pr                    | 2.9  | 2.8  | 2.4  | 1.5  | 2.1  | 2    | 1.8  | 2.2  | 3    | 2.2  | 2.3  | 2.5  | 1.9  | 3.2  | 2.4  | 3.8  | 2.9  | 2.1  | 2.1  | 1.6  |
| Nd                    | 10.6 | 9.5  | 8.1  | 4.6  | 7.4  | 6.5  | 5.8  | 6.7  | 10.4 | 7.8  | 7.5  | 8.8  | 6.3  | 11.5 | 8.5  | 13.2 | 10.2 | 6.5  | 6.5  | 4.9  |
| Sm                    | 1.7  | 1.5  | 1.3  | 0.7  | 1.2  | 0.9  | 0.9  | 1    | 1.7  | 1.3  | 0.9  | 1.4  | 0.9  | 1.8  | 1.4  | 2.5  | 1.7  | 0.9  | 1    | 0.8  |
| Eu                    | 0.3  | 0.2  | 0.2  | 0.1  | 0.2  | 0.2  | 0.1  | 0.2  | 0.3  | 0.2  | 0.2  | 0.3  | 0.2  | 0.3  | 0.2  | 0.3  | 0.3  | 0.2  | 0.2  | 0.2  |
| Gd                    | 1.3  | 1.1  | 1    | 0.6  | 0.9  | 0.6  | 0.7  | 0.7  | 1.2  | 0.9  | 0.7  | 1    | 0.7  | 1.2  | 1.1  | 2    | 1.2  | 0.7  | 0.8  | 0.6  |
| Tb                    | 0.2  | 0.2  | 0.2  | 0.1  | 0.1  | 0.1  | 0.1  | 0.1  | 0.2  | 0.1  | 0.1  | 0.2  | 0.1  | 0.2  | 0.2  | 0.4  | 0.2  | 0.1  | 0.1  | 0.1  |
| Dy                    | 0.9  | 0.9  | 0.9  | 0.5  | 0.7  | 0.6  | 0.5  | 0.6  | 1.8  | 0.6  | 0.5  | 1    | 0.5  | 0.9  | 0.8  | 3.2  | 0.9  | 0.6  | 0.9  | 0.7  |
| Ho                    | 0.2  | 0.2  | 0.2  | 0.1  | 0.1  | 0.1  | 0.1  | 0.1  | 0.4  | 0.1  | 0.1  | 0.2  | 0.1  | 0.2  | 0.2  | 0.7  | 0.2  | 0.1  | 0.2  | 0.2  |
| Er                    | 0.6  | 0.6  | 0.6  | 0.4  | 0.4  | 0.4  | 0.4  | 0.4  | 1.6  | 0.4  | 0.3  | 0.7  | 0.3  | 0.5  | 0.6  | 2.9  | 0.5  | 0.4  | 0.7  | 0.6  |
| Tm                    | 0.1  | 0.1  | 0.1  | 0.1  | 0.1  | 0.1  | 0.1  | 0.1  | 0.3  | 0.1  | 0.1  | 0.2  | 0.1  | 0.1  | 0.1  | 0.6  | 0.1  | 0.1  | 0.2  | 0.1  |
| Yb                    | 0.9  | 0.8  | 0.9  | 0.7  | 0.6  | 0.7  | 0.6  | 0.8  | 2.7  | 0.5  | 0.4  | 1.2  | 0.5  | 0.7  | 0.9  | 5    | 0.6  | 0.8  | 1.3  | 1.3  |
| Lu                    | 0.1  | 0.1  | 0.2  | 0.2  | 0.1  | 0.1  | 0.1  | 0.2  | 0.4  | 0.1  | 0.1  | 0.2  | 0.1  | 0.1  | 0.2  | 0.8  | 0.1  | 0.2  | 0.2  | 0.3  |
| Parameters and ratios |      |      |      |      |      |      |      |      |      |      |      |      |      |      |      |      |      |      |      |      |
| P                     | -64  | -39  | -54  | -59  | -46  | -57  | -56  | -62  | -38  | -53  | -37  | -46  | -23  | -13  | -46  | -19  | 3    | -67  | -70  | -45  |
| Q                     | 188  | 208  | 222  | 182  | 203  | 178  | 192  | 182  | 198  | 184  | 187  | 200  | 241  | 241  | 196  | 224  | 244  | 189  | 200  | 162  |
| B                     | 9.0  | 12.8 | 11.0 | 11.8 | 6.4  | 7.8  | 9.8  | 11.3 | 7.5  | 6.6  | 7.5  | 12.1 | 11.4 | 13.0 | 10.1 | 14.5 | 15.0 | 11.6 | 10.0 | 7.3  |
| A                     | 13.8 | 38.1 | 30.2 | -6.7 | 22.2 | 13.4 | -3.0 | -3.9 | 11.8 | 8.8  | 10.2 | 16.5 | 48.0 | 44.3 | 16.7 | 41.5 | 59.2 | -7.6 | 0.5  | -1.5 |
| Th/U                  | 3.1  | 2.3  | 2.0  | 1.5  | 4.2  | 2.1  | 1.3  | 0.9  | 3.6  | 4.1  | 6.8  | 3.6  | 6.2  | 4.1  | 2.0  | 2.7  | 4.1  | 1.9  | 1.3  | 0.8  |
| Rb/Sr                 | 1.6  | 2.3  | 2.3  | 5.4  | 2.1  | 3.9  | 5.7  | 3.9  | 3.5  | 1.8  | 4.4  | 1.9  | 2.8  | 1.9  | 3.0  | 1.7  | 2.1  | 4.0  | 3.2  | 5.3  |
| Nb/Ta                 | 8.1  | 8.3  | 8.2  | 9.1  | 8.6  | 8.8  | 8.9  | 10.4 | 9    | 11.4 | 10.6 | 7.7  | 17.7 | 9.9  | 8.5  | 9.3  | 10.1 | 10.6 | 9.6  | 8.1  |
| Zr/Hf                 | 21.5 | 22.6 | 19.5 | 19.1 | 24.5 | 21.1 | 18.4 | 19.7 | 23.3 | 22.2 | 24.4 | 26.4 | 24.4 | 23.4 | 22.1 | 25.4 | 23.5 | 20.0 | 20.6 | 16.9 |

The peraluminosity is calculated as the difference between the total amount of Al present in the rock and the amount of Al bound to the feldspars:  $A = Al - (Na + K + 2Ca)$ , calculated in cations. This index indicates the excess or the deficiency of Al with respect to the quantity needed to make the feldspars. The granites have compositions varying from slightly metaluminous ( $A = -7$ ) to peraluminous ( $A = 62$ ). The peraluminous compositions correspond mineralogically to the presence of Al-rich biotite and small amounts of muscovite. The four most peraluminous samples (W<sub>2</sub>-5, 6, 8 and 9) present the lowest Na contents (3.2 to 2.6 wt% Na<sub>2</sub>O, instead of more than 4 wt% for the other samples) and the highest ignition losses (1.9 to 3.1 wt% instead of about 1 wt% for the other samples).

These features indicate an argillic alteration of the plagioclase in these samples. The metaluminous samples tend to have the highest Ca contents (0.7 to 1.1 wt% CaO), without a corresponding increase of the ignition loss indicating the presence of Ca silicates and the absence of a significant carbonate contribution (Figure 3). Quartz and feldspars are located at the origin in this diagram and represent the eutectic composition of the granite system. The differentiation parameter  $B = Fe + Mg + Ti$ , which also represents a coloration index of the rock. The granite are leucocratic with low B-parameter values ( $B < 15$ ).

The granites of the three drill holes tend to define three distinct magmas batches in the A-B and Q-P diagrams (Figure 3 and Figure 4). The samples of drill hole W3 have all very low peraluminosity for very leucocratic compositions in the A-B diagram and are among the richest in plagioclase for low quartz contents in the Q-P diagram. Samples from W1 form a trend parallel to the one defined by the samples from the W3 drilling with higher average peraluminosity. Two samples have higher A parameter due to clay alteration especially for W1-2 (lower Na<sub>2</sub>O content and higher ignition loss). In the Q-P diagram the samples define a fractionation trend with simultaneous increase of quartz and K-feldspar content. Sample W1-3 is slightly silicified. The W2 drill hole hosts the 4 samples with the highest degree of clay alteration as discussed above and well evidenced in the A-B and Q-P diagrams (Figure 3 and Figure 4). The other samples define a different than the two other drill holes with a decrease of the A parameter (20 to 10) with a decrease of the B parameter (13 to 4). These samples are also the richest in K-feldspar for similar quartz contents.

The compositions and the global trends defined in the A-B and Q-P diagram (Figure 3 and Figure 4) correspond to highly fractionated high-K calc-alkaline granites. Initially derived from metaluminous sources they become slightly peraluminous by extreme fractionation of Ca-rich, Al-poor or absent minerals (amphiboles and or

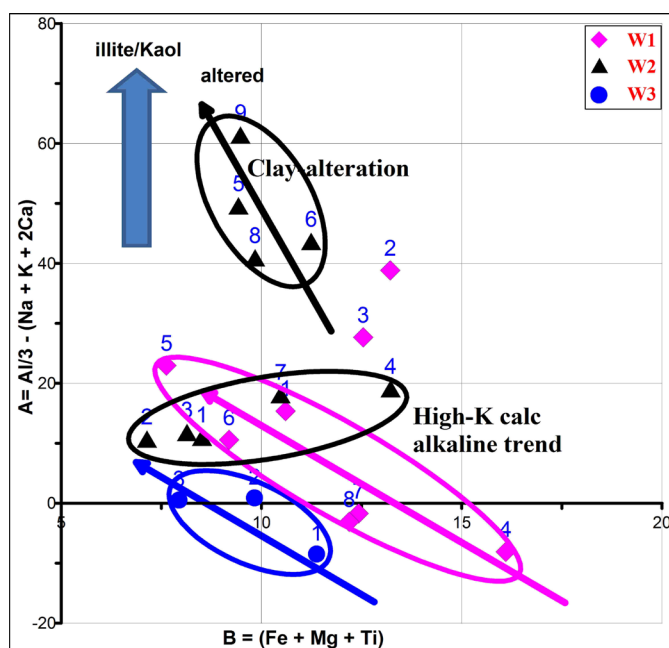


**Figure 3.** Variation of the peraluminous index (A) with fractionation index (B), for the two-mica granite at G. El Sela shear zone. A-B mine-ralogical-chemical diagram, from [23] parameters in thousands of cations.

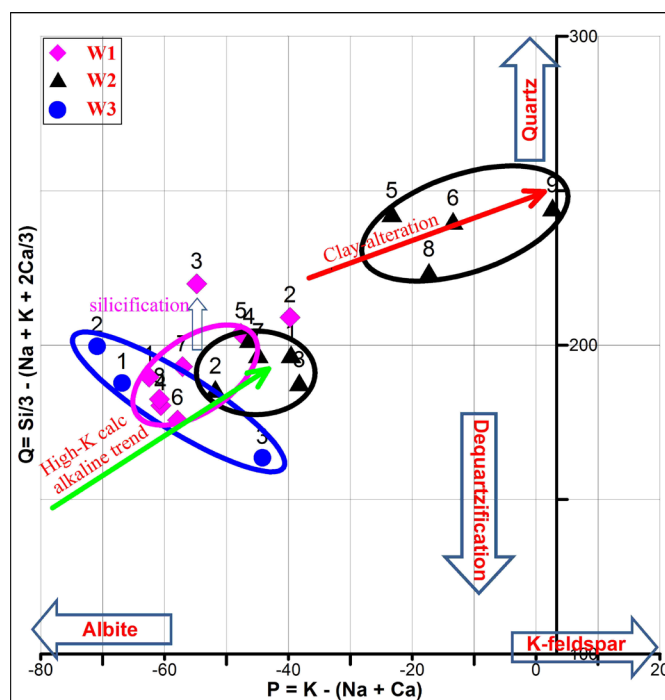


**Figure 4.** Variation of the K-feldspar/albite (P parameter) versus quartz contents (Q parameter) for the two-mica granite at El Sela shear zone. Q-P mineralogical-chemical diagram from [23] parameters in thousands of cations.

pyroxenes), and possible assimilation of peraluminous crustal material during their ascent, and/or incipient alteration of the feldspars in K-micas or clay minerals.

## 5.2. Trace Elements

The granites from the El Sela shear zone are found to be rich in most large ion lithophile elements (LILE; Ba, Rb, Sr) and high field strength elements (HFSE; Y, Zr and Nb) **Table 1**. The biotite ± muscovite granite is moderately rich in Th (16 to 29 ppm) and U (3 to 33 ppm). The highest U values are observed in borehole W1 and W3. Sample W1-8 at a depth of 63 m has the highest Th and U contents (29 and 33 ppm respectively) (**Figure 5**). Most samples of the W2 drilling tend to follow a simultaneous enrichment in Th and U, with a Th/U ratio of 4. However, the Th richest samples (W2-3 and 5) are slightly depleted in uranium (Th/U > 4). Sample 5 shows a clay alteration which may explain the U loss but not samples 3. Sample 7 tends to be enriched in U (Th/U = 2). Th samples from drill hole W1 plot along a well-defined trend with increasing Th and U and decreasing Th/U, sample W1-8 being the richest in U and Th with a Th/U below 1 indicates the possible presence of uraninite. This trend seems to reflect magmatic fractionation. However, the three Th and U richest samples (W1-4, 7 and 8) are the less fractionated in the A-B diagram (**Figure 3**). The three samples of drill hole W3 define a hydrothermal U enrichment trend with low Th/U (<2).

In the Nb versus Sn diagram (**Figure 6**) most samples from each drill hole form well defined groups with increasing Sn and Nb contents from W2 to W1 and W3, although W3 is the less peraluminous group of samples (**Figure 3**). Sample W1-4 is anomalously enriched in Sn relatively to Nb, whereas samples W1-8 and W3-3 are anomalously enriched in Nb. All the enrichments remain however limited (up to 32 ppm Nb and 6 ppm Sn).

In the diagram Zr versus Hf two groups of granites (one for most samples from W2 and another with the samples from W1 and W3) are well defined with distinct Zr/Hf ratios (**Figure 7**). Granites from the drill hole W2 show the lowest Hf contents.

Nb and Ta are very well correlated (**Figure 8**). They also define three granite groups corresponding to the three drill holes with increasing Nb and Ta concentrations from W2 to W1 and W3, as for the Sn-Nb correlation, with a nearly constant Nb/Ta ratio of 10. However, the highest Ta contents do not exceed 5 ppm.

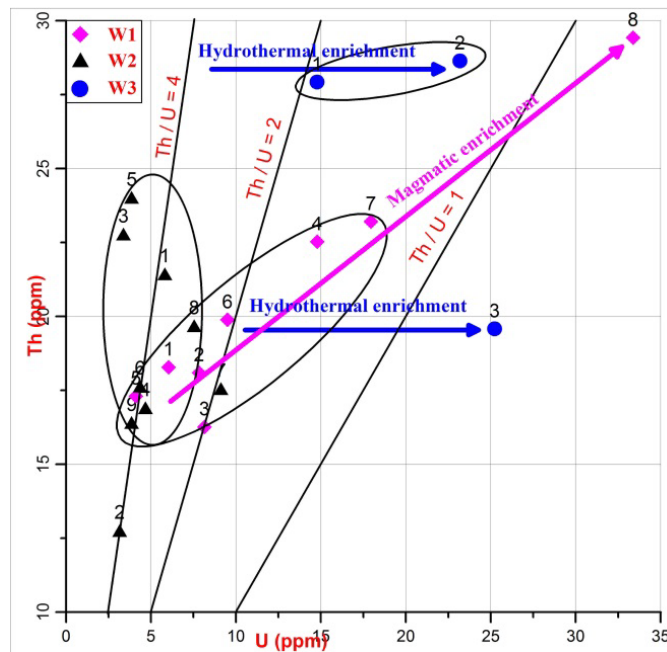


**Figure 5.** U-Th relationships of the studied boreholes at G. El Sela shear zone.

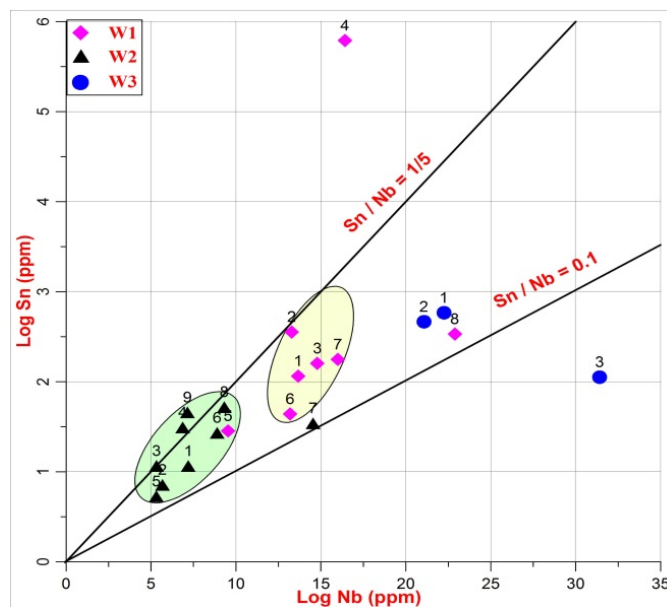


**Figure 6.** Nb-Sn relationships of the studied boreholes at G. El Sela shear zone.

The concentrations of trace elements are normalized to the primitive mantle [24] are represented as spider diagrams (Figure 9). The El Sela granites show enrichment of large ion lithophile elements (LILE; Rb, Ba, Sr) and high field strength elements (HFSE; Y, Zr, Nb) and a marked moderate level of Ba, Ce and Ti in the three boreholes which are typical of subduction related magmas [25] [26] (Figure 9).

### 5.3. Rare Earth Elements

The El Sela granite has variable total REE contents: 44 to 98 ppm in samples W<sub>1</sub>-6 and W<sub>2</sub>-8 respectively

(Table 1). The chondrite-normalized REE patterns enrichment strong fractionation of light rare earth elements (LREE) ( $5.34 < (La/Sm)_N < 12.9$ ) and flat to reversely fractionated heavy rare earth elements (HREE) ( $4.6 < (Ga/Yb)_N < 58.3$ ) (Figure 9 and Figure 10). The negative Eu anomaly observed in the granites from the three  $W_1$ ,  $W_2$  and  $W_3$  drill hole. Two samples from  $W_2$  present an enrichment in the heaviest REE and Y with a

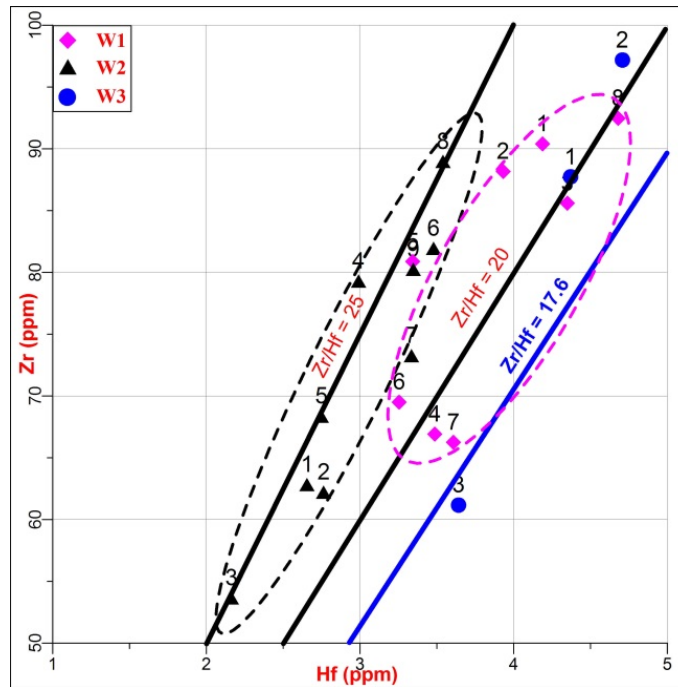


Figure 7. Hf (ppm)-Zr (ppm) relationship for the granites of the G. El Sela shear zone, and show the reference Zr/Hf isovalent ratio of 17.6.

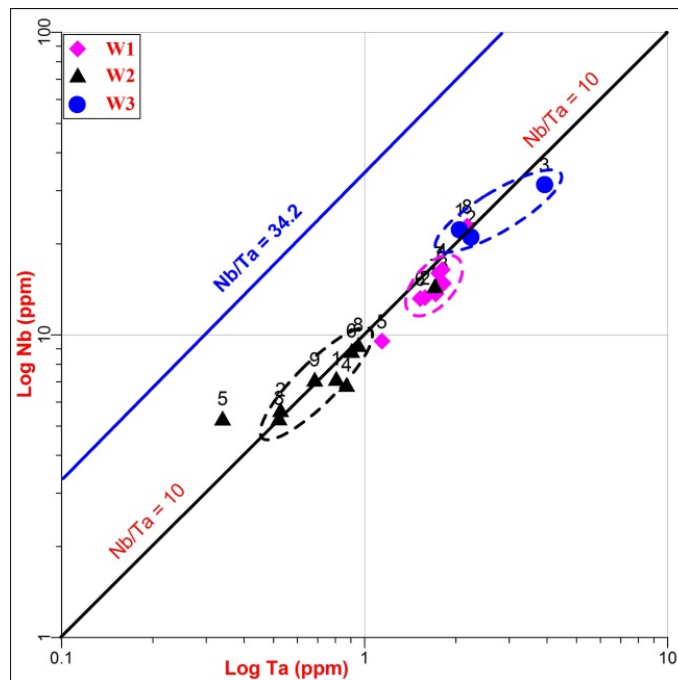
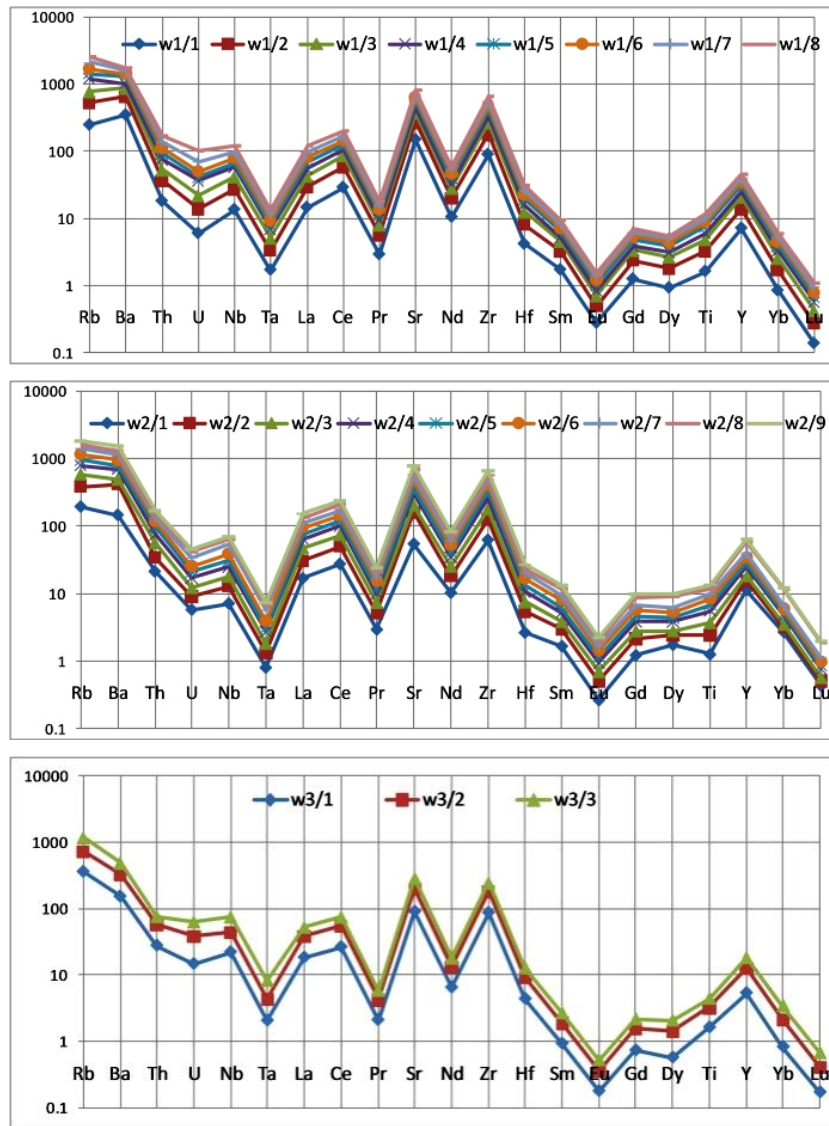


Figure 8. Nb (ppm) - Ta (ppm) for the granites of the G. El Sela shear zone, and show the reference Nb/Ta isovalent ratio of 34.2.



**Figure 9.** Primitive-mantle-normalized multi-elements spider diagrams (normalization values are from [24]) for the El Sela granite.

strongly reverse HREE fractionation, indicating the abundance of a HREE-rich mineral, which may correspond to xenotime. The negative Eu suggests that plagioclase was an early fractionating phase.

## 6. Mineral Chemistry

Scanning electron microscope (SEM) and electron microprobe analyses (EMPA) were used to identify the nature of the sulfides and Nb-Ta-, Zr-Hf-, REE-, Th-, U-bearing minerals in the El Sela granite (Figure 11) and Table 2 to Table 4.

### 6.1. Sulfides

Pyrite, chalcopyrite, arsenopyrite, galena, and sphalerite, occur as disseminations and fracture-fillings in mineralized smoky and red jasperoid veins, dolerite and microgranite dikes, in the El Sela granites illustrated by Figure 11(a). Magnetite, hematite, illmenite, rutile and apatite are also spatially associated with the sulfide minerals. Pyrite ( $\text{FeS}_2$ ) is the most common sulfide mineral which occurs as well developed octahedral crystals.

Pyrite is preserved in the samples from the drillings and seems to control the deposition of uraninite, branne-

**Table 2.** Electron microprobe analyses of Ti-, Nb-Ta-, Zr-Hf-, REE-minerals from the El Sela granite.

| S. No.                         | W3-3<br>-C3 | W3-2<br>-C2 | W1-7<br>C10-4 | W1-4<br>C1-2 | W2-5<br>-C3 | W2-9<br>-C2 | W1-4<br>C4-1 | W1-4<br>C4-2 | W1-7<br>C10-3 | W2-5<br>-C3 | W2-9<br>-C10 | W3-3<br>-C4 | W3-3<br>-C4 | W3-3<br>-C4             | W1-7<br>-C6-2 | W1-7<br>-C6-3 | W3-3<br>-C3 |
|--------------------------------|-------------|-------------|---------------|--------------|-------------|-------------|--------------|--------------|---------------|-------------|--------------|-------------|-------------|-------------------------|---------------|---------------|-------------|
| depth m.                       | 43          | 30          | 62            | 53           | 26          | 44          | 53           | 53           | 62            | 26          | 44           | 43          | 43          | 43                      | 62            | 62            | 43          |
| oxides                         | Beta-fite   | rutile      |               |              |             | Zircon      |              |              |               |             |              |             |             | REE-rich<br>uranthorite | columbite     |               |             |
| SiO <sub>2</sub>               | 1.56        | 0           | 0.5           | 0.56         | 0.73        | 4.6         | 30.4         | 26.6         | 32.4          | 29.1        | 32.3         | 29.5        | 27.7        | 28.8                    | 19.0          | 11.4          | 0.09        |
| P <sub>2</sub> O <sub>5</sub>  | 0.05        | 0           | 0             | 0            | 0           | 0           | 0.43         | 0.85         | 0.42          | 0.56        | 0.45         | 0.3         | 0.71        | 0.44                    | 1.04          | 1.1           | 0           |
| SO <sub>2</sub>                | 0           | 0           | 0             | 0            | 0           | 0           | 0            | 0            | 0             | 0           | 0.01         | 0           | 0           | 0                       | 0.16          | 0             | 0           |
| CaO                            | 2           | 0.34        | 0.18          | 0.29         | 0.04        | 0.2         | 0.85         | 1.48         | 0.1           | 0.44        | 0.02         | 0.6         | 1.21        | 0.68                    | 7.81          | 7.7           | 0.14        |
| TiO <sub>2</sub>               | 46.3        | 85.8        | 64.1          | 90.1         | 92.7        | 82.3        | 0.1          | 0.1          | 0             | 0.13        | 0            | 0           | 0.08        | 0                       | 0.15          | 0.02          | 11          |
| MnO                            | 0.24        | 0.05        | 1.05          | 0.08         | 0.05        | 0.02        | 0.63         | 0.38         | 0.07          | 0.1         | 0            | 0.49        | 0.36        | 0.46                    | 0.08          | 0.03          | 9.76        |
| FeO                            | 8.48        | 4.4         | 21.6          | 1.47         | 0.39        | 5.78        | 1.2          | 0.87         | 0.22          | 2.5         | 0.03         | 1.41        | 1.26        | 1.53                    | 1.89          | 0.13          | 7.6         |
| Y <sub>2</sub> O <sub>3</sub>  | 0.1         | 0.04        | 0             | 0            | 0           | 0.03        | 0            | 0.89         | 0             | 0           | 0            | 0           | 0.44        | 0                       | 1.11          | 1.58          | 0.84        |
| ZrO <sub>2</sub>               | 0.64        | 0.04        | 0.07          | 0.15         | 0           | 0.03        | 59.9         | 54.6         | 63.9          | 59.9        | 66.0         | 59.5        | 49.3        | 60.4                    | 2.84          | 0             | 0.55        |
| Nb <sub>2</sub> O <sub>5</sub> | 22.8        | 7.56        | 1.61          | 1.18         | 0.51        | 0.94        | 0            | 0            | 0             | 0           | 0            | 0           | 0           | 0                       | 0.28          | 0.04          | 62.3        |
| SnO                            | 0.08        | 0.3         | 0             | 0            | 0           | 0           | 0            | 0.01         | 0             | 0           | 0.01         | 0           | 0           | 0                       | 0             | 0             | 0.15        |
| La <sub>2</sub> O <sub>3</sub> | 0           | 0           | 0             | 0            | 0           | 0           | 0            | 0            | 0.02          | 0           | 0            | 0           | 0           | 0.02                    | 4.51          | 4.02          | 0           |
| Ce <sub>2</sub> O <sub>3</sub> | 0.15        | 0.26        | 0.2           | 0.28         | 0.27        | 0.27        | 0            | 0.04         | 0             | 0           | 0.01         | 0           | 0           | 0.08                    | 7.74          | 7.3           | 0           |
| Nd <sub>2</sub> O <sub>3</sub> | 0.08        | 0           | 0.03          | 0            | 0           | 0           | 0.01         | 0.13         | 0.02          | 0           | 0.12         | 0           | 0.15        | 0.07                    | 2.24          | 2.16          | 0.03        |
| Yb <sub>2</sub> O <sub>3</sub> | 0.08        | 0           | 0             | 0            | 0           | 0.02        | 0            | 0.4          | 0.12          | 0.01        | 0            | 0.16        | 0.43        | 0                       | 0.02          | 0             | 0.28        |
| HfO <sub>2</sub>               | 0.55        | 1.22        | 0.9           | 1.23         | 1.33        | 1.27        | 2.24         | 3.09         | 1.68          | 1.49        | 1.26         | 2.2         | 10.9        | 1.7                     | 0             | 0             | 0.1         |
| Ta <sub>2</sub> O <sub>5</sub> | 2.7         | 0.33        | 0.03          | 0.03         | 0           | 0.05        | 0.28         | 0.13         | 0.34          | 0.22        | 0.33         | 0.37        | 0.56        | 0.29                    | 0             | 0             | 2.91        |
| PbO                            | 0           | 0           | 0             | 0            | 0           | 0           | 0            | 0            | 0             | 0           | 0            | 0           | 0           | 0                       | 0.11          | 0.02          | 0           |
| ZnO                            | n.d         | n.d         | 0.02          | 0.06         | 0           | 0           | 0            | 0            | 0             | 0           | 0            | n.d         | n.d         | n.d                     | 0             | 0             | n.d         |
| Al <sub>2</sub> O <sub>3</sub> | n.d         | n.d         | 0.26          | 0.43         | 0.24        | 1.3         | 0.21         | 0.56         | 0.03          | 0.1         | 0            | n.d         | n.d         | n.d                     | 7.52          | 0.66          | n.d         |
| ThO <sub>2</sub>               | 5.8         | 0           | 0.06          | 0.03         | 0           | 0.04        | 0.04         | 0.54         | 0.03          | 0.6         | 0            | 0.27        | 0.68        | 1.22                    | 25.9          | 42.2          | 0.2         |
| UO <sub>2</sub>                | 1.57        | 0           | 0.27          | 1.21         | 0.01        | 0           | 1            | 1.57         | 0             | 0.79        | 0.17         | 1.33        | 2.24        | 1.61                    | 1.3           | 1.19          | 0.75        |
| Total                          | 93.**       | 100.**      | 91            | 97           | 96          | 97          | 97           | 92           | 99            | 96          | 101          | 96          | 96          | 97                      | 84            | 80            | 97          |

rite, pitchblende and coffinite at the margin of the crystals. In the El Sela shear zone the cavities left after pyrite dissolution are by uranophane and autunite because of the alteration of the pyrite and primary U minerals by meteoric fluids [28].

Sulfides are more effective reductant because sulfur can act as reducing agent where one mole of pyrite can reduce six more uranium than Fe<sup>+2</sup> [29].

## 6.2. Ti-, Nb-Ta-, Zr-Hf-, REE-Mineralization

Rutile, fluorite, zircon, monazite, LREE-carbonates, columbite and betafite have been also identified by SEM and EMPA analyses.

Rutile is common mineral in most samples from the El Sela granite. It occurs as angular to subangular, elong-

**Table 3.** Electron microprobe analyses (EMPA) of Th-, U-minerals from the El Sela granite.

| S. No.                         | W <sub>2-9</sub> -C <sub>10</sub> | W <sub>1-7</sub> -C <sub>10-2</sub> | W <sub>2-5</sub> -C <sub>3</sub>   | W <sub>2-5</sub> -C <sub>3</sub>   | W <sub>2-5</sub> -C <sub>3</sub> | W <sub>2-9</sub> -C <sub>10</sub> | W <sub>2-9</sub> -C <sub>10</sub> | W <sub>1-7</sub> -C <sub>6-1</sub> | W <sub>1-7</sub> -C <sub>10-1</sub> | W <sub>3-3</sub> -C <sub>4</sub>   | W <sub>3-2</sub> -C <sub>1</sub> | W <sub>3-2</sub> -C <sub>1</sub> | W <sub>3-2</sub> -C <sub>2</sub> | W <sub>3-2</sub> -C <sub>3</sub> |
|--------------------------------|-----------------------------------|-------------------------------------|------------------------------------|------------------------------------|----------------------------------|-----------------------------------|-----------------------------------|------------------------------------|-------------------------------------|------------------------------------|----------------------------------|----------------------------------|----------------------------------|----------------------------------|----------------------------------|----------------------------------|----------------------------------|
| depth m.                       | 44                                | 62                                  | 26                                 | 26                                 | 26                               | 44                                | 44                                | 62                                 | 62                                  | 43                                 | 30                               | 30                               | 30                               | 30                               | 30                               | 30                               | 30                               |
| oxides                         | thorite                           | phosphothorite                      |                                    |                                    |                                  |                                   | uranothorite                      |                                    |                                     |                                    | brannerite                       |                                  |                                  |                                  |                                  |                                  |                                  |
| SiO <sub>2</sub>               | 33.73                             | 11.5                                | 14.2                               | 16.3                               | 8.77                             | 21.1                              | 28.7                              | 17.9                               | 16.8                                | 20.8                               | 6.8                              | 6.08                             | 13.35                            | 3.02                             | 11.4                             | 5.48                             | 2.85                             |
| P <sub>2</sub> O <sub>5</sub>  | 1.48                              | 1.51                                | 15.11                              | 4.84                               | 10.28                            | 8.68                              | 10.61                             | 0.47                               | 0.28                                | 1.85                               | 0.14                             | 0.03                             | 0.29                             | 0.18                             | 0.61                             | 0.22                             | 0.07                             |
| SO <sub>2</sub>                | 0.07                              | 0.08                                | 0.34                               | 0.05                               | 0.21                             | 0.34                              | 0.08                              | 0.07                               | 0.08                                | 0.05                               | 7.76                             | 0                                | 0                                | 0                                | 0                                | 0                                | 0                                |
| CaO                            | 1.96                              | 5.29                                | 7.85                               | 2.61                               | 4.84                             | 8.82                              | 12.95                             | 1.52                               | 1.73                                | 2.63                               | 2.42                             | 3                                | 3.42                             | 3.19                             | 1.51                             | 4.69                             | 1.75                             |
| TiO <sub>2</sub>               | 0.04                              | 0.1                                 | 0                                  | 0                                  | 0.01                             | 0                                 | 0                                 | 0                                  | 0.04                                | 0.26                               | 22.9                             | 31.3                             | 17.2                             | 31.4                             | 41.6                             | 22.7                             | 62.8                             |
| MnO                            | 0.07                              | 0.02                                | 0                                  | 0.05                               | 0.01                             | 0.03                              | 0.01                              | 0.01                               | 0                                   | 0.09                               | 0.19                             | 0.72                             | 0.13                             | 0.35                             | 0.07                             | 0.69                             | 0.34                             |
| FeO                            | 3.12                              | 0.67                                | 0.57                               | 0.59                               | 0.6                              | 0.55                              | 0.49                              | 0.11                               | 0.06                                | 1.18                               | 7.25                             | 2.07                             | 0.78                             | 2.48                             | 2.17                             | 0.9                              | 0.99                             |
| Y <sub>2</sub> O <sub>3</sub>  | 0.2                               | 1.22                                | 0.88                               | 1.97                               | 3                                | 1.53                              | 1.24                              | 0.77                               | 0.06                                | 2.23                               | 0                                | 1.23                             | 1.56                             | 0                                | 1.44                             | 0                                | 0                                |
| ZrO <sub>2</sub>               | 0.6                               | 1.45                                | 0.07                               | 0                                  | 0                                | 1.69                              | 2                                 | 0                                  | 0.26                                | 11.6                               | 2.72                             | 1.37                             | 9.32                             | 1.63                             | 3.96                             | 1.66                             | 0.64                             |
| Nb <sub>2</sub> O <sub>5</sub> | 0.19                              | 0.09                                | 0                                  | 0.15                               | 0                                | 0.01                              | 0                                 | 0.09                               | 0                                   | 0.3                                | 2.21                             | 3.54                             | 0.3                              | 1.59                             | 0.74                             | 1.67                             | 0.96                             |
| La <sub>2</sub> O <sub>3</sub> | 0.01                              | 0.28                                | 0.28                               | 0.04                               | 0.06                             | 0.01                              | 0.03                              | 0                                  | 0                                   | 0                                  | 0                                | 0                                | 0                                | 0                                | 0                                | 0                                | 0                                |
| Ce <sub>2</sub> O <sub>3</sub> | 0                                 | 0.56                                | 0.03                               | 0.22                               | 0.28                             | 0.09                              | 0.11                              | 0.11                               | 0.04                                | 0.15                               | 0.17                             | 0.53                             | 0.21                             | 0.14                             | 0.23                             | 0.15                             | 0.25                             |
| Nd <sub>2</sub> O <sub>3</sub> | 0.38                              | 0.47                                | 0.52                               | 0.82                               | 0.27                             | 0.66                              | 0.29                              | 0.24                               | 0.13                                | 0.31                               | 0.01                             | 0.43                             | 0.08                             | 0.07                             | 0.08                             | 0                                | 0.07                             |
| Yb <sub>2</sub> O <sub>3</sub> | 0.03                              | 0                                   | 0.23                               | 0                                  | 0.09                             | 0.19                              | 0                                 | 0                                  | 0                                   | 0.36                               | 0.09                             | 0.37                             | 0.21                             | 0                                | 0.21                             | 0                                | 0                                |
| HfO <sub>2</sub>               | 0                                 | 0                                   | 0                                  | 0                                  | 0                                | 0                                 | 0                                 | 0                                  | 0                                   | 0                                  | 0                                | 0                                | 0                                | 0                                | 0                                | 0                                | 0.03                             |
| Ta <sub>2</sub> O <sub>5</sub> | 0.06                              | 0                                   | 0.03                               | 0                                  | 0                                | 0                                 | 0.07                              | 0                                  | 0                                   | 0                                  | 0                                | 0                                | 0                                | 0                                | 0                                | 0                                | 0                                |
| PbO                            | 0.12                              | 0.17                                | 0.09                               | 0.09                               | 0.13                             | 0.09                              | 0                                 | 0.31                               | 0.75                                | 0.12                               | 0                                | 0                                | 0                                | 0.63                             | 0                                | 0                                | 0                                |
| ZnO                            | 0                                 | 0                                   | 0                                  | 0                                  | 0                                | 0                                 | 0.02                              | 0                                  | 0.02                                | n.d                                | n.d                              | n.d                              | n.d                              | 0                                | 0                                | 0                                | 0                                |
| Al <sub>2</sub> O <sub>3</sub> | 3.23                              | 0.16                                | 1.62                               | 0.25                               | 0.49                             | 2.85                              | 6.34                              | 0.11                               | 0.03                                | n.d                                | n.d                              | n.d                              | n.d                              | n.d                              | 0.44                             | 0.22                             | 0.46                             |
| ThO <sub>2</sub>               | 48.1                              | 63.5                                | 54.4                               | 62.7                               | 61.9                             | 45.1                              | 27.5                              | 52.0                               | 53.5                                | 33.0                               | 1.4                              | 2.19                             | 1.28                             | 0.66                             | 0.57                             | 0.59                             | 0.18                             |
| UO <sub>2</sub>                | 0                                 | 0                                   | 0.22                               | 0.84                               | 2.1                              | 0.19                              | 0.45                              | 18.4                               | 14.5                                | 11.4                               | 36.4                             | 39.0                             | 39.8                             | 36.8                             | 26.3                             | 49.1                             | 15.7                             |
| Total                          | 93.4                              | 87.1                                | 96.4                               | 91.5                               | 93.0                             | 91.9                              | 90.9                              | 92.1                               | 88.4                                | 86.5                               | 90.5                             | 91.9                             | 88.5                             | 82.1                             | 91.4                             | 88.1                             | 87.1                             |
| S. No.                         | W <sub>3-2</sub> -C <sub>10</sub> | W <sub>3-2</sub> -C <sub>10</sub>   | W <sub>1-7</sub> -C <sub>8-3</sub> | W <sub>1-4</sub> -C <sub>1-3</sub> | W <sub>3-2</sub> -C <sub>5</sub> | W <sub>3-2</sub> -C <sub>5</sub>  | W <sub>3-3</sub> -C <sub>2</sub>  | W <sub>3-3</sub> -C <sub>2</sub>   | W <sub>1-4</sub> -C <sub>2-1</sub>  | W <sub>1-4</sub> -C <sub>2-4</sub> | W <sub>3-3</sub> -C <sub>4</sub> | W <sub>3-3</sub> -C <sub>4</sub> | W <sub>3-3</sub> -C <sub>6</sub> |
| depth m.                       | 30                                | 30                                  | 62                                 | 53                                 | 30                               | 30                                | 53                                | 53                                 | 53                                  | 53                                 | 43                               | 43                               | 43                               | 43                               | 43                               | 43                               | 43                               |
| oxides                         | brannerite                        |                                     |                                    | coffinite                          |                                  |                                   |                                   | uraninite                          |                                     |                                    |                                  | pitchblende                      |                                  |                                  |                                  |                                  |                                  |
| SiO <sub>2</sub>               | 6.86                              | 5.23                                | 1.8                                | 25.1                               | 18.6                             | 12.0                              | 16.0                              | 22.2                               | 6.89                                | 3.06                               | 9.45                             | 13.55                            | 4.08                             | 4.69                             | 3.56                             | 4.31                             | 1.05                             |
| P <sub>2</sub> O <sub>5</sub>  | 0.03                              | 0.11                                | 0.08                               | 0.06                               | 1.16                             | 2.28                              | 0.66                              | 0.72                               | 0.25                                | 0.17                               | 1.06                             | 1.56                             | 0.15                             | 0.1                              | 0.11                             | 0.43                             | 0.13                             |
| SO <sub>2</sub>                | 0                                 | 0                                   | 0                                  | 0                                  | 1.28                             | 0.41                              | 0.25                              | 3.41                               | 0.09                                | 1.09                               | 1.88                             | 0.02                             | 0                                | 1.3                              | 0.04                             | 0.06                             | 6.68                             |
| CaO                            | 1.96                              | 2                                   | 2.14                               | 2.17                               | 2.15                             | 1.84                              | 7.66                              | 2.63                               | 3.95                                | 7.56                               | 6.59                             | 3.78                             | 4.44                             | 4.18                             | 5.28                             | 3.36                             | 3.36                             |
| TiO <sub>2</sub>               | 28.2                              | 41.4                                | 45.1                               | 3                                  | 0.26                             | 0.28                              | 0.2                               | 0.17                               | 1.47                                | 1.1                                | 0.63                             | 2.4                              | 0                                | 0                                | 0                                | 0                                | 0                                |
| MnO                            | 0.09                              | 0.19                                | 0.49                               | 0.36                               | 0.01                             | 0                                 | 1.62                              | 0.14                               | 0.81                                | 0.69                               | 0.44                             | 0.44                             | 0.12                             | 0.04                             | 0.17                             | 0.08                             | 0.13                             |
| FeO                            | 1.6                               | 1.14                                | 2.1                                | 3.04                               | 2.28                             | 1.06                              | 4.59                              | 3.36                               | 11.65                               | 4.69                               | 3.66                             | 1.02                             | 1.92                             | 3.98                             | 1.58                             | 0.47                             | 6.51                             |

## Continued

|                                |      |      |      |       |      |      |      |      |      |      |      |      |      |      |      |      |      |
|--------------------------------|------|------|------|-------|------|------|------|------|------|------|------|------|------|------|------|------|------|
| Y <sub>2</sub> O <sub>3</sub>  | 0.04 | 0    | 0    | 0     | 3.34 | 3.77 | 1.53 | 1.7  | 0    | 0    | 2.02 | 2.96 | 0.06 | 0.08 | 0.14 | 0.96 | 0.22 |
| ZrO <sub>2</sub>               | 1.7  | 0.87 | 1.65 | 2.92  | 3    | 3.13 | 6.34 | 5.91 | 8.29 | 4.34 | 7.14 | 8.65 | 0.01 | 0    | 0.16 | 0.25 | 0.05 |
| Nb <sub>2</sub> O <sub>5</sub> | 3.99 | 4.41 | 1    | 0.83  | 0.13 | 0.1  | 1.82 | 1.51 | 1.99 | 2.08 | 2.29 | 2.12 | 0    | 0.03 | 0.34 | 0.48 | 0.08 |
| SnO                            | 0    | 0    | 0    | 0     | 0    | 0    | 0    | 0    | 0    | 0    | 0    | 0    | 0    | 0    | 0    | 0    | 0    |
| La <sub>2</sub> O <sub>3</sub> | 0    | 0    | 0    | 0     | 0.07 | 0.02 | 0.03 | 0    | 0    | 0.02 | 0.06 | 0    | 0.1  | 0.13 | 0.13 | 0.09 | 0.07 |
| Ce <sub>2</sub> O <sub>3</sub> | 0.3  | 0.28 | 0.45 | 0.13  | 0.28 | 0.26 | 0.17 | 0.09 | 0.29 | 0.21 | 0.3  | 0.26 | 0.5  | 0.5  | 0.45 | 0.54 | 0.52 |
| Nd <sub>2</sub> O <sub>3</sub> | 0.03 | 0.19 | 0.21 | 0     | 0.26 | 0.24 | 0.2  | 0    | 0.02 | 0    | 0.21 | 0.36 | 0.21 | 0.04 | 0.23 | 0.34 | 0.16 |
| Yb <sub>2</sub> O <sub>3</sub> | 0.01 | 0    | 0.1  | 0     | 0.62 | 0.47 | 0.44 | 0.36 | 0.03 | 0    | 0.27 | 0.44 | 0    | 0    | 0.07 | 0.24 | 0    |
| HfO <sub>2</sub>               | 0    | 0    | 0    | 0     | 0    | 0    | 0    | 0    | 0    | 0    | 0    | 0    | 0    | 0    | 0    | 0    | 0    |
| Ta <sub>2</sub> O <sub>5</sub> | 0    | 0    | 0    | 0     | 0    | 0    | 0    | 0    | 0    | 0    | 0    | 0    | 0    | 0    | 0    | 0    | 0    |
| PbO                            | 0    | 0    | 0    | 0.92  | 0    | 0    | 0.34 | 0.36 | 2.13 | 1.16 | 2.35 | 0    | 0.73 | 0.69 | 0.38 | 0.15 | 0.47 |
| ZnO                            | 0.05 | 0    | 0    | 0     | 0    | n.d  | n.d  | n.d  | 0    | 0    | n.d  |
| Al <sub>2</sub> O <sub>3</sub> | 0.24 | 0.21 | 0.64 | 12.13 | 1.99 | 0.49 | n.d  | n.d  | 1.19 | 0.38 | n.d  |
| ThO <sub>2</sub>               | 1.9  | 2.17 | 0.2  | 1.1   | 1.31 | 2.33 | 1.29 | 0.71 | 2.97 | 1.65 | 1.1  | 2.37 | 0    | 0    | 0    | 0.03 | 0    |
| UO <sub>2</sub>                | 43.7 | 33.4 | 36.7 | 34.1  | 56.8 | 61.7 | 32.6 | 27.8 | 47.2 | 63.0 | 51.2 | 49.2 | 76.8 | 77.8 | 82.2 | 78.8 | 80.4 |
| Total                          | 90.7 | 91.7 | 92.6 | 85.8  | 93.5 | 90.4 | 75.8 | 71.1 | 89.2 | 91.2 | 90.5 | 89.1 | 89.2 | 93.6 | 94.8 | 90.7 | 99.9 |

Table 4. The main characteristics El Sela granite in the vicinity of the main shear zone.

| Borehole No.               | W1  | W2   | W3  |
|----------------------------|---|--|---|
| Rock types                 | <ul style="list-style-type: none"> <li>0 - 12 m: wadi deposits.</li> <li>12 - 63 m: biotite ± muscovite granite.</li> </ul>   | <ul style="list-style-type: none"> <li>0 - 44 m: biotite ± muscovite granite.</li> </ul> | <ul style="list-style-type: none"> <li>0 - 43 m: biotite ± muscovite granite.</li> </ul>  |
| Hydrothermal alteration    | biotite highly altered into ferrichlorite pennite), muscovitization, albitization, sericitization, kaolinization and argillization.                                   |  |   |
| Sulfides                   | Pyrite, arsenopyrite, chalcopyrite, galena and sphalerite   |  |   |
| Nb-Ti-, Zr-Hf-, F-minerals | Columbite, betafite, rutile, zircon   | Columbite, rutile, zircon  | Columbite, betafite, rutile, zircon, fluorite   |
| REE-minerals               | Allanite, LREE carbonate  | Allanite   | Allanite  |
| Th-minerals                | Thorite   | Thorite, phosphothorite with apatite   | Thorite   |
| U-Th-minerals              | uranothorite  |  |   |
| U-minerals                 | <ul style="list-style-type: none"> <li>Brannerite, coffinite, uraninite and pitchblende</li> <li>W1-4 and W1-7 samples at depth 53 and 62 m, respectively.</li> </ul> |  | <ul style="list-style-type: none"> <li>Brannerite, coffinite, uraninite and pitchblende</li> <li>W3-2 and W3-3 samples at depth 30 and 43 m, respectively.</li> </ul> |

gated, cylinder and -like grains of reddish brown to blackish brown colors associated with zircon, fluorite, monazite, uranothorite, and uraninite (Figures 11(b)-(d)). The EMPA analyses indicate that the rutile has 0.39 - 8.48 wt.% Fe<sub>2</sub>O<sub>3</sub>, 0.51 to 22.78 Nb<sub>2</sub>O<sub>3</sub> and up to 2.7 wt.% Ta, 5.8 wt.% Th, and 1.57 wt.% U (Table 3). It would be interesting in which samples the highest concentration of each element has been found to interpret the whole rock geochemistry.

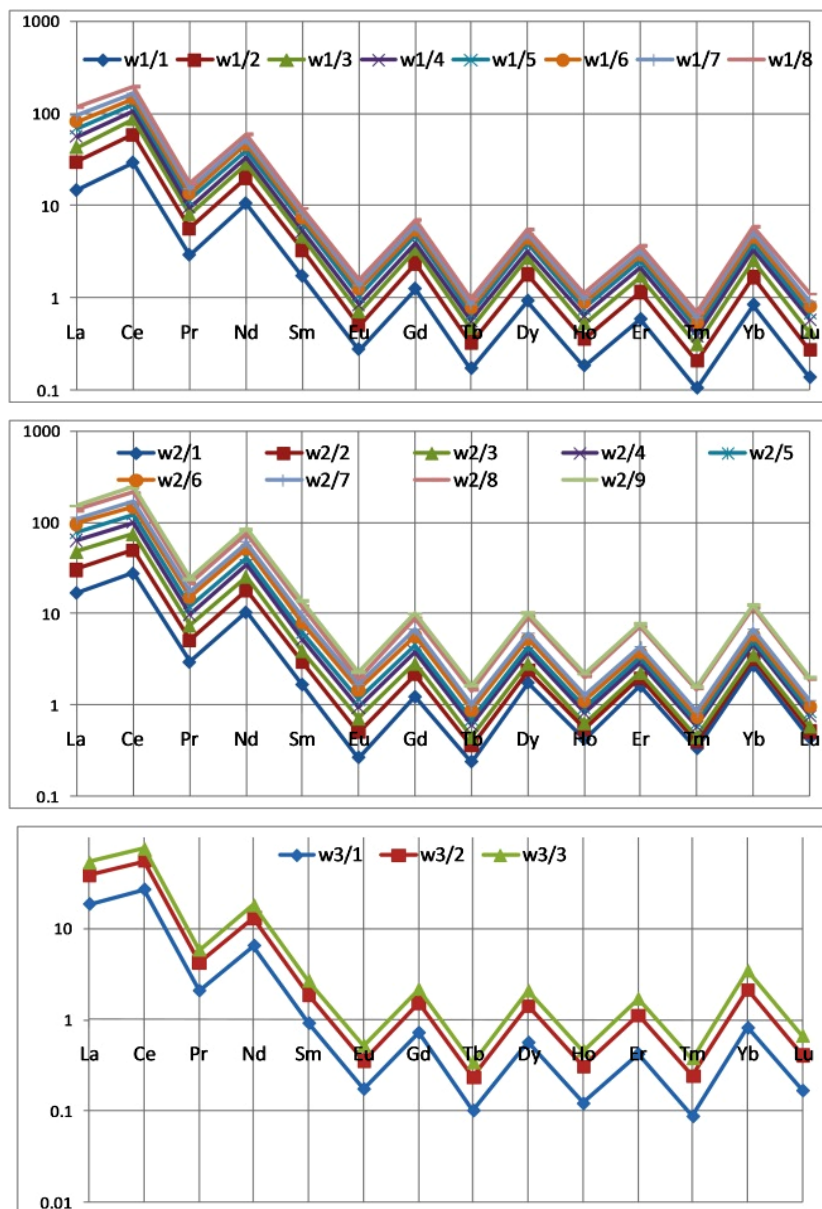


**Figure 10.** Chondrite-normalized REE patterns (normalization values are from [27] for the El Sela granite.

Zircon is generally included as idiomorphic crystals (Figure 11(c)) variably enriched in hafnium (Table 2) ( $1.26 < \text{HfO}_2 < 10.87$  wt.%),  $\text{UO}_2$  (up to 2.23 wt.%) and  $\text{ThO}_2$  up to (up to 1.22 wt.%). Similar Hf enrichment has been observed in Rare Metal Granites such as at Cinovec with 3 to 4 wt.%  $\text{HfO}_2$  [30].

Uranothorite crystals occur as brownish red and orange crystals, isotropic because of their metamictisation.  $\text{SiO}_2$  and  $\text{ThO}_2$  (25.93 - 42.2 wt.%) concentrations are quite variable and analytical total are low due to the strong metamictization of the crystals (Table 2). Uranium concentrations are low and frequently below the EPMA detection limit (Table 3 & Figure 11(e)).

Columbite [(Fe, Mn)(Nb, Ta, Ti) $\text{O}_4$ ] occurs as dark gray to black color, flattened, prismatic, massive subhedral to euhedral crystals (Figure 11(f)). The SEM-BSE image and EPMA analyses shows that it is a ferro-columbite with 7.59 wt.%  $\text{Fe}_2\text{O}_3$ , 11 wt.%  $\text{TiO}_2$ , 9.76 wt.% MnO with minor amount of U and Th 0.75 and 0.2 wt.% respectively, (Table 2).

Betafite (Ca, U) $_2$ (Ti, Nb, Ta) $_2\text{O}_6$ (OH) is detected under the SEM-BSE image (Figure 11(f)) as Nb-Ti-bearing

mineral occurring as subhedral mineral in the boreholes W1 and W3 of two-mica granite. The obtained results confirm from a chemical analyses of the studied betafite minerals by SEM analyses, the major elements are included Nb<sub>2</sub>O<sub>5</sub> vary from (12.4% to 21.4%), TiO<sub>2</sub> vary from (13.2% to 45.9%), FeO vary from (1.9 to 8.3 wt.%), Ta<sub>2</sub>O<sub>5</sub> reach 4.6 wt.% and MnO reach 1.24 wt.%. It obvious that betafite has higher U concentration reaches 22.5, 26.95 and 31.9 wt.% with lower content in W3-3-C3 1.14 wt.%.

Thorite, phosphothorite, uranothorite, brannerite, coffinite, uraninite and pitchblende have been identified by SEM and EPMA analyses (**Figure 11** & **Table 3**). Thorite and uranothorite is rare in the El Sela granites but phosphothorite was observed in the granites from the W1 and W2 drill hole. Thorite-group minerals form euhedral to subhedral crystals, black to brown colors and enclosed in biotite, quartz, zircon and monazite. Based on SEM and EMPA analyses four types of thorite-group minerals can be distinguished; thorite, Zr-rich thorite, phosphothorite and uranothorite (**Figure 11(b)**, **Figure 11(c)**, **Figure 11(e)**; **Table 3**). The total of the analyses of all these minerals is low (close to 90 wt% or lower) indicating their strong metamictisation and hydration. ThO<sub>2</sub> contents in thorite vary from 20.1 to 48.8 wt.% and SiO<sub>2</sub> from 5.1 to 33.7 wt.% **Table 3**. SEM analyses reveal locally Zr-rich thorite the W<sub>1</sub>-1 and W<sub>2</sub>-3 drill holes with 5 to 8 wt.% ZrO<sub>2</sub>. The occurrence of thorite within zircon crystal cores indicates a thorite analysis may be contaminated by the enclosing zircon crystal. Phosphothorite composition exhibits a wide range of U, Zr, Y, LREE, Ca and P contents (**Table 4**). ThO<sub>2</sub> varies from 27.5 to 63.5 wt.%, P<sub>2</sub>O<sub>5</sub> from 1.5 to 15.1 wt.%, CaO vary from 2.6 to 12.95 wt.%, Y<sub>2</sub>O<sub>3</sub> vary from 0.8 to 3 wt.% and SiO<sub>2</sub> vary from 8.7 to 28.6 wt.% **Table 3**.

Uranothorite (U, Th)SiO<sub>4</sub> is interstitially associated with iron oxides and/or found as numerous subhedral to anhedral inclusions in zircon. The EPMA analyses indicate that UO<sub>2</sub> contents may reach 18.4 wt% and Y<sub>2</sub>O<sub>3</sub> 2.23 wt% composition of zircon up to 11.6 wt.% **Table 3**.

Ti-U oxides are the most U minerals in the El Sela granites (**Figure 11(g)** & **Table 3**). They generally form aggregates along the periphery of pyrite or occur as pseudomorphs of former Ti-minerals such as ilmenite and titanite El Sela granite. The major elements composition is variable: TiO<sub>2</sub> to 62.8 wt.% and UO<sub>2</sub> range from 15.7 to 49.1 wt.%. Up to 9.32 wt.% ZrO<sub>2</sub> may also be present. Brannerite is associated with uraninite along pyrite crystals at depths 53 m and 43 m in boreholes W1 and W<sub>3</sub>, respectively.

Uranium oxides occur in granites samples (W3-1, -2, -3 and W1-4) as minute crystals filling micro-fractures and/or associated with pyrite, rutile and fluorite or with other U-minerals such as brannerite (**Figure 11(d)**, **Figure 11(g)**). ThO<sub>2</sub> content of uraninite vary from (1.1 to 3 wt.%), for PbO contents from 1.16 to 2.35 wt.%, P<sub>2</sub>O<sub>5</sub> contents from 0.17 to 1.56 wt.% and CaO contents from 3.8 to 7.6 wt.%. Also, minor amounts of LREE and Y are present (**Table 3**). Under reducing conditions, uraninite may be altered to coffinitization, with loss of radiogenic Pb and Y with HREE, [31]. The variable amounts of SiO<sub>2</sub> indicate Si diffusion in the structure along fractures at the beginning of coffinitization.

EMPA analyses show the major elements are SiO<sub>2</sub> vary from (11.98 to 25.13 wt.%) and UO<sub>2</sub> vary from (27.48 to 61.73 wt.%) correspond to the composition of coffinite **Table 3** and **Figure 11(h)**.

EPMA analyses show a wide variation of the pitchblende composition which exhibit very weak zoning and occurs as botryoidally form or vein surrounded metallic sulfides especially pyrite (**Figure 11(i)**, **Figure 11(j)**). Most samples have no Th or traces (up to 0.03 wt.%) **Table 3** but significant contents of SiO<sub>2</sub> (up to 4.69 wt.%), CaO (5.28 wt.%), Y<sub>2</sub>O<sub>5</sub> (0.96 wt.%), ZrO<sub>2</sub> (0.25 wt.%), Nb<sub>2</sub>O<sub>5</sub> (0.48 wt.%), PbO (0.73%) and REE (0.30 wt.%). Moreover the trace elements in pitchblende may occur in the form of minute inclusions (galena, pyrite, sphalerite etc.) or as amorphous mixtures such as Ca<sup>2+</sup>, Pb<sup>2+</sup>, Th<sup>4+</sup> and REE<sup>3+</sup> which have similar ionic size to that of U<sup>4+</sup>. The high FeO contents in some samples (3.98 or 6.51 wt.%) is not attributed to substitution for U because of the large difference in atomic radii (Fe<sup>3+</sup> = 0.64 Å; U<sup>4+</sup> = 0.97 Å). It may correspond to some inclusions such as hematite and pyrite. The U contents fluctuate between 76.84 wt.% and 82.15 wt.% in relation with the effect of the substitutions of other elements. Silica contents range between 1.05 to 4.69 wt.%.

The granite from the El Sela shear zone area are enriched in the lighter isovalents Nb and Zr relatively to the heavier isovalents Ta, Hf elements. The lower Zr/Hf ratio is in accordance with the presence of Hf-rich zircons (3 to 4 wt.% HfO<sub>2</sub>) (**Table 4**).

## 7. Radon Mapping

Uranium exploration has been aided by the identification of radon anomalies near the surface [32]. These anomalies can detect hidden uranium deposits that are too deep to be seen with gamma rays from the uranium

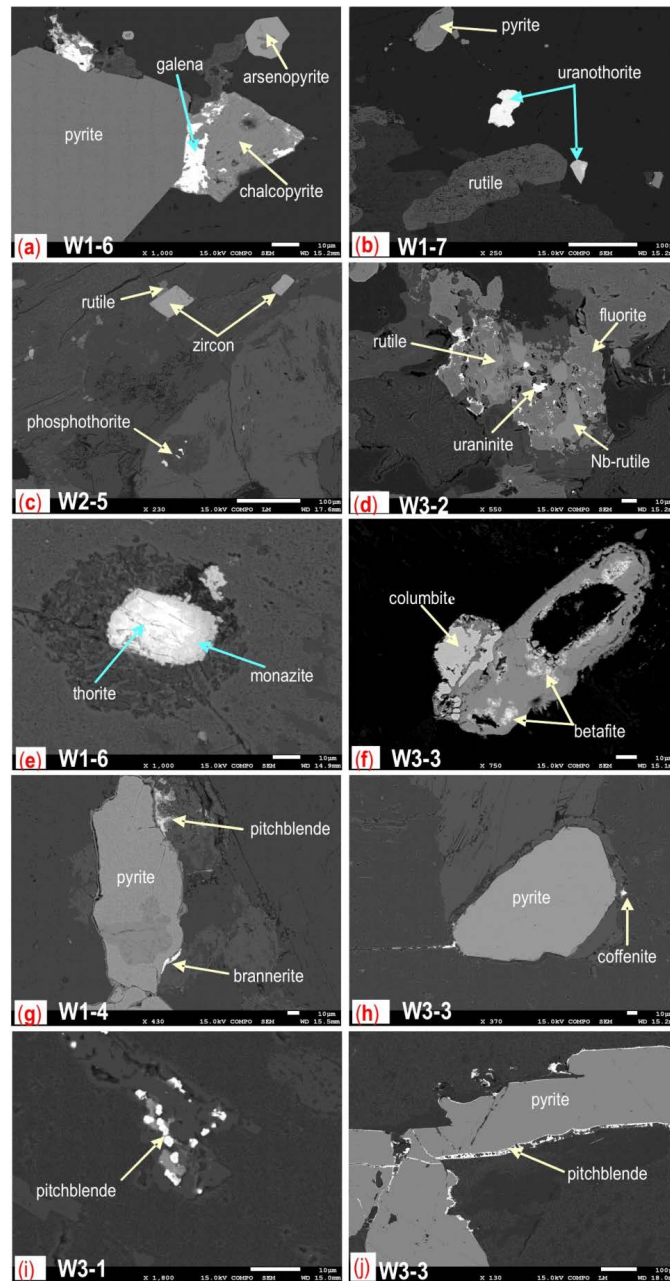


**Figure 11.** Representative back-scattered electron microscopy (BSEM) images of different minerals from El Sela granites. (a) Pyrite, chalcopyrite, arsenopyrite and galena. (b) Association of uranothorite, rutile and pyrite. (c) Rutile along periphery of zircon with phosphothorite. (d) Uraninite enclosed between fluorite and rutile-(Nb). (e) Monazite crystal enclosed thorite. (f) Nb-minerals (columbite and betafite). (g) Uraninite and brannerite along the periphery of pyrite. (h) Pyrite surrounded by coffinite. (i) Botryoidal pitchblende. (j) Veinlet of pitchblende at the margin of pyrite crystals.

daughter products or with normal surface geochemical techniques, which analyze uranium or radium. Radon, a relatively mobile gas, can originate from deeply buried deposits and gaseous or aqueous movement to the surface can transport it where it can be readily detected [33]. However a great care has to be taken in the interpretation as radon emanations because it may migrate relatively far from its source.

Shear zones, faults and joints are the main conducts for radon emanations to the surface especially for structure controlled deposits. Radon anomalies can be detected over deeply buried uranium mineralization. At the present time it is known that ore bodies at depths of 100 m to 200 m can generally be detected and that depth of up to 300 meters are possible in very favorable circumstances [33].

Obviously, the cluster distribution map of radon shows that the radon activity varies along shear zone over a wide range that lies between  $960 \text{ Bq/m}^3$  to  $300,300 \text{ Bq/m}^3$  (Figure 12). The distribution of radon activity 3D-image map (Figure 13) shows clearly that the radon emission is heterogeneous along shear zone with about seven strong anomalies (Figure 13). The largest of these anomalies, which is located on the eastern side of the study area occupies large area of about  $200 \text{ m}^2$  and reaches a radon activity act of  $296,000 \text{ Bq/m}^3$ . In the west direction another anomaly with a smaller extension presents the highest radon activity from the study area with  $300,300 \text{ Bq/m}^3$ . This anomaly is characterized by the existence of visible surficial uranium mineralization that is represented by uranophane and autunite.

The western part of the study area is occupied with an anomaly covering an area of medium intensity between the two previous two anomalies but the radon activity is up to half their values which is approximately  $150,000 \text{ Bq/m}^3$ . In the middle of the study area there is a small radon anomaly reaches about  $200,000 \text{ Bq/m}^3$ .

## 8. Geophysical Signatures of Sela Geologic Cross-Sections

The variations of K, eU and eTh concentrations and their ratios, beside the VLF-EM and magnetic data are illustrated along two cross sections nearly perpendicular to the Sela shear zone as shown in Figure 14 & Figure 15. Potassium reached its highest values ( $4\% \pm 1\%$ ) in two mica granites and decrease abruptly in the shear main zone with less than  $0.5\%$ . The eTh variations reflect contrasts between the biotite granite and the two-mica granite. The biotite granite produces some of the highest eTh values (up to  $50 \text{ ppm}$ ) and exhibits strong internal magmatic zonation. The two-mica granite tends to have lower Th concentrations. The lowest values ( $<3 \text{ ppm}$ ) occur in the shear zone. eU profile is mainly characterized by one anomaly, related to the shear zone and reaching  $>600 \text{ ppm}$ . The remaining rock units in the study area show low uranium concentrations ( $1 \text{ to } 20 \text{ ppm}$ ), but with three small anomalies which coincide with thorium anomalies. The shear zone is also logically characterized by high eU/eTh and eU/K ratios (up to 7 and 90). Field investigations have shown that uranium has been strongly concentrated along fractures. Uraninite has been located along the margins and discrete radioactive sources. In case of the two-mica granites, there is no appreciable variation in eU versus eU/eTh ratio. This indicates that uranium in initially as uraninite in the two mica granite; U may have been leached by weathering in the surface samples which are analyzed by gamma spectrometry. The coincident Th and U anomalies within the biotite granite, may indicate U-Th minerals refractory to weathering.

The VLF-EM profiles (Figure 14 and Figure 15) show a marked increase of conductivity directly over the shear zone indicating vertical or steeply dipping sources. The VLF survey does not allow differentiating the biotite granite from the two-mica granite. The location of the VLF anomalies also correspond to a strongly positive

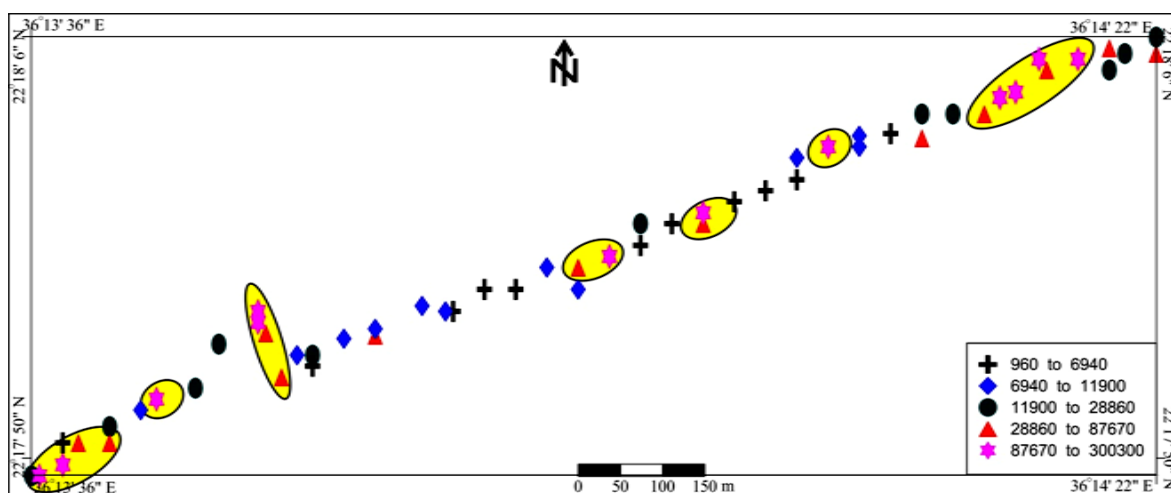
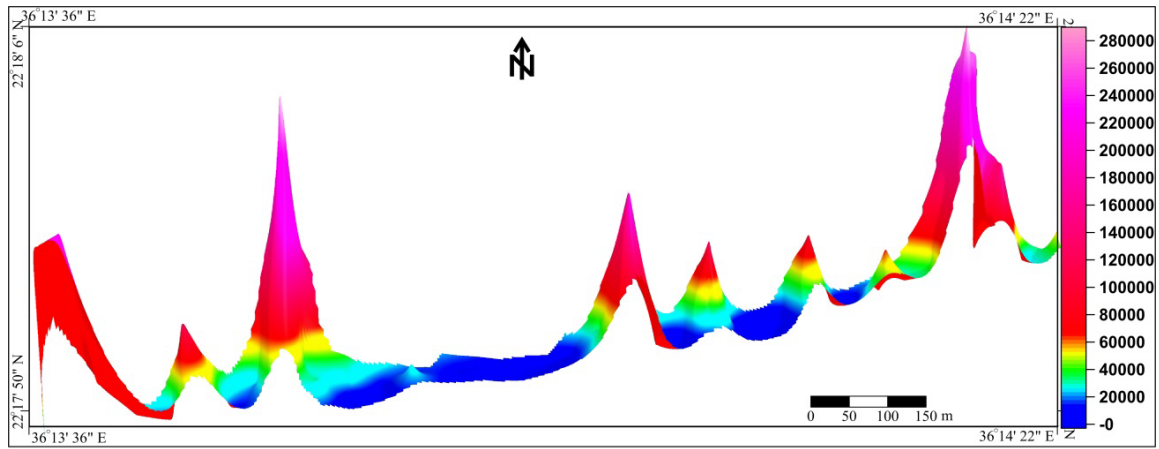
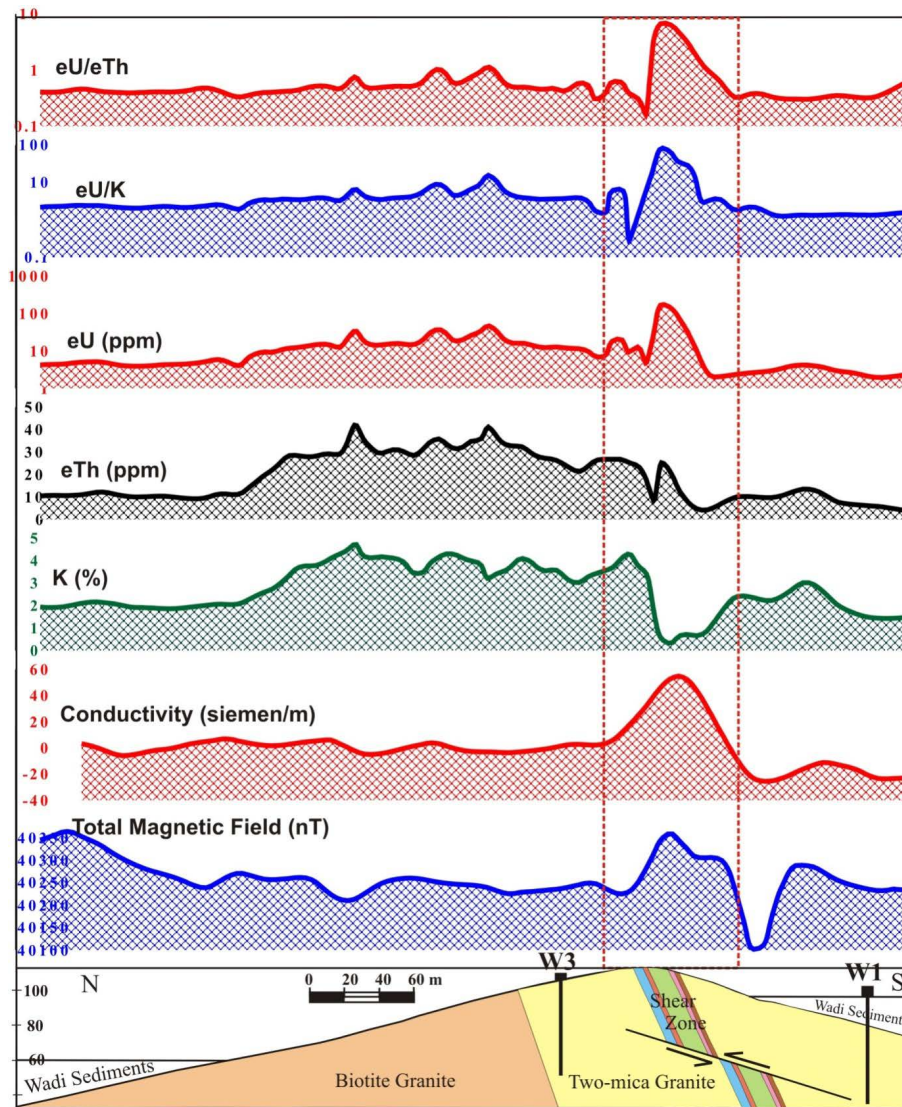


Figure 12. Radon concentration classed map ( $\text{Bq/m}^3$ ) of Sela area, S E D, Egypt.



**Figure 13.** Radon activities 3D-image map ( $Bq/m^3$ ) of Sela area, S E D, Egypt.



**Figure 14.** Stacked profiles for radio elements, magnetic field and conductivity across the two wells W1 and W3 of Sela area, Southern Eastern Desert, Egypt.

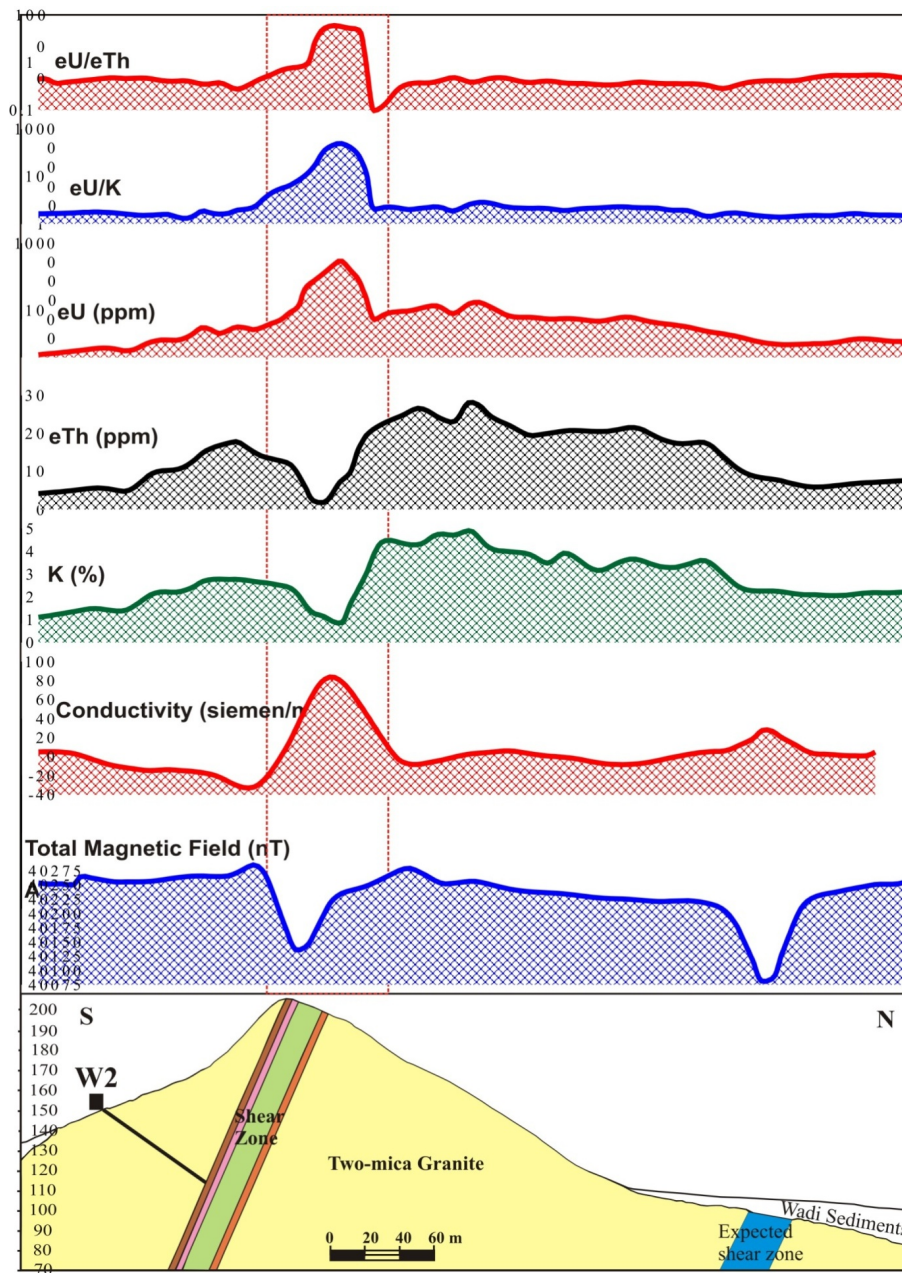


**Figure 15.** Stacked profiles for radio elements, magnetic field and conductivity across the two well W2 of Sela area, Southern Eastern Desert, Egypt.

magnetic anomaly for the first profile passing through the W1 and W3 drill holes, probably caused by the lamprophyre which may have high magnetite content. Immediately to the East of the magnetic high, there is a sharp magnetite low which may correspond to a strongly oxidized zone at the southern margin of the Sela Shear Zone.

In the second profile passing through the drill hole W2, above the Sela shear zone, the conductivity high correspond to the opposite of the preceding profile to a low in the total magnetic field, narrower than the conductivity high. Such a low magnetic field should correspond to a zone were the Fe-Ti bearing minerals have been oxidized or pyritized. A similar total magnetic field low is observed to the south of the Sela shear zone covered by sand, but is not associated with a conductivity high this indicate the causative body is located at depth more than 30m where the sense detection of VLF technique. The magnetic field over the granitic rocks and the wadi sediments is characterized by low magnetic signatures.

## 9. Discussion and Conclusion

### 9.1. Uranium Fertility of the El Sela Granite

The El Sela granite complex is composed of biotite and biotite ± muscovite granites. The three samples of drill holes have only intersected the biotite ± muscovite granites. Geochemically, the El Sela granites are very leucocratic, meta- to slightly per-aluminous and enriched in large ion lithophile elements (LILE: Ba, Rb and Sr), high field strength elements (HFSE: Y, Zr and Nb), light rare earth elements (LREE) mostly hosted in allanite, Th mostly hosted in uranothorite and allanite and uranium partly hosted in magmatic Th-bearing uraninite, but relatively poor in Ta, Sn, Be and heavy rare earth elements (HREE). Most of them have a negative Eu anomaly. Their characteristics correspond to those of A2-type granites (high-K calc-alkaline granites).

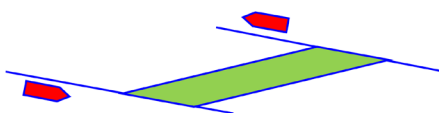
During most geological processes the chondritic ratios of the isovalent elements Nb/Ta ( $34.2 \pm 0.3$ ) and Zr/Hf ( $17.6 \pm 1$ ) are constant [34]. However Nb and Ta can fractionate in peraluminous magmas because of the higher solubility of Ta (tantalite) relatively to Nb (columbite) in such melts [35]. Nb-Ta, Nb-Ti rich minerals are represented by columbite and betafite.

The Th/U ratios of the El Sela granites vary from about 6, indicating uranium leaching, to 0.8 indicating late magmatic and/or hydrothermal enrichment. 6 samples have Th/U ratios below 2 indicating that magmatic or hydrothermal U-oxides may be present as the main U-bearing minerals. Th-bearing uraninite has been identified in two samples (W1-53 with 15 ppm U and 23 ppm Th and W3-43 with 25 ppm U and 20 ppm). Uraninite may have been present in other shallower samples but may have been leached by hydrothermal and/or meteoric fluids. The presence of uraninite in the El Sela granite indicates that it can represent a good uranium source, even if uranothorite was not sufficiently metamict to liberate uranium at the time of the circulation of the hydrothermal fluids.

### 9.2. The Hydrothermal Ore System

Two sets of structures are observed in the El Sela granite: a major E-W to ENE-WSW shear zone and N-S to NNE-SSW set of fault associated with different types of contemporaneous magmatic injections. These structures are reactivated several times in association with succession fluid circulations leading to the deposition of a series of quartz generations and U mineralization.

The main shear zone at G. El Sela is trending ENE-WSW and steeply dipping from  $70^\circ$  to  $85^\circ$  to the south. This trend has been reactivated many times by NNW-SSE extensional stress field, however to know that a detailed structural study would be necessary. The stress field may be transtensional with opening of tension gashes filled by the microgranite in the eastern part of the shear zone and filled by microgranite and dolerite dikes with white quartz and reddish to black jasperoid veins.



The main shear zone is affected by hydrothermal alteration as ferrugination, silicification, albitation, epsyenitization, illitization and fluoritization with U-mineralization as hexavalent U minerals visible at the surface. The N-S strike slip sinistral fault cross-cut the ENE-WSW shear zone main trend. The width of the mineralized part of the shear zone varies from 3 to 40 m and is developed over a length of 1.5 km but reached 6 km in the east of G. El Sela area.

One of the aims of the present study is to detect U-mineralization in the drilled core samples and also to identify the depth of the reduced zone where the primary hydrothermal U-mineralization may be present.

The continuation of the uranium mineralization at depth is evidenced by the Track Etch Survey along the El Sela main shear zone with radon emission from 960 to 300,300 Bq/m<sup>3</sup>.

The  $\gamma$ -ray spectrometric profiles across the Sela shear zone indicate the strong increase of eU and, eU/eTh and eU/K ratios and a decrease of eTh and eK anomaly in relation with the enrichment of the shear zone in quartz. The strong direct increase of eU/eTh ratio is typical of hydrothermal uranium enrichment with no mobility of Th.

The VLF-EM profiles show marked high positive conductivity correlated with the shear zone within the gra-

nitic body, indicating higher fracturation and clay mineral content of the shear zone. The magnetic profile passing through W1 and W3 shows clearly an increase of total magnetic field above the El Sela shear zone associated with a magnetic low at its southern margin. To the opposite the magnetic profile passing through W<sub>2</sub> showed only a strong magnetic low above the El Sela shear zone. Therefore, the association of spectrometric, radon, magnetic and electrical conductivity anomalies for the Sela shear zone clearly identifies the uranium-anomalous zones which can be selected for more drilling.

The occurrence of U-oxides along the margin of the pyrite crystals may indicate that they have played a role on the reduction of U<sup>6+</sup> from the uranyl ion (UO<sub>2</sub><sup>2+</sup>) dissolved in the hydrothermal fluids into U<sup>4+</sup> which precipitates as, brannerite, coffinite and pitchblende. Pb tends to migrate outside the uranium mineral structure [36]. In the present study Pb released from U-oxides commonly forms galena.

The occurrence of brannerite indicates a first phase of U remobilization at relatively high temperature, brannerite being stable above 250°C - 300°C. The U-oxides are also locally altered to coffinite [31]. Pitchblende occurs as botryoidal form or vein deposited on pyrite.

## References

- [1] Cuney, M. (2009) The Extreme Diversity of Uranium Deposits. *Mineralium Deposita*, **44**, 3-9. <http://dx.doi.org/10.1007/s00126-008-0223-1>
- [2] IAEA (2009) World Distribution of Uranium Deposits (UDEPO) with Uranium Deposit Classification. IAEA, Vienna, IAEA-TECDOC-1629, 117 p.
- [3] Cuney, M., Le fort, P. and Wang, Z.X. (1984) Uranium and Thorium Geochemistry and Mineralogy in the Manaslu leucogranite (Nepal, Himalaya). *Geology of Granites and Their Metallogenic Relations (Proceedings of a Symposium)*, Nanjing, 1982, University Sciences Editions, 853-873.
- [4] Poty, B., Cuney, M. and Friedrich, M. (1986) Uranium Deposits Spatially Related to Granites in the French Part of the Hercynian Orogeny, Vein Type Uranium Deposits. IAEA-TECDOC-361, IAEA, Vienna, 215-246.
- [5] Friedrich, M.H., Cuney, M. and Cregu, G. (1989) Uranium Enrichment Processes in Peraluminous Magmatism. International Atomic Energy Agency (IAEA)-TC-571/2.11-35.
- [6] Rameshbabu, P.V. (1999) Rare Metal and Rare Earth Pegmatites of Central India. Special Issue on Rare Metal and Rare Earth Pegmatites of India. *Exploration and Research*, **12**, 7-52.
- [7] Pal, D.C., Mishra, B. and Bernhardt, H.J. (2007) Mineralogy and Geochemistry of Pegmatite-Hosted Sn-, Ta-Nb- and Zr-Hf-Bearing Minerals from the Southeastern Part of the Bastar-Malkangiri Pegmatite Belt, Central India. *Ore Geology Reviews*, **30**, 30-55. <http://dx.doi.org/10.1016/j.oregeorev.2005.10.004>
- [8] Jiashu, R. and Zehong, H. (1982) Forms of Uranium Occurrence and Its Distribution in Uraniferous Granites. In: *Geology of Granites and Their Metallogenic Relations*, Sciences Press, Beijing, 621-635.
- [9] Ibrahim, M.E. (1986) Geologic and Radiometric Studies on Um Ara Granite Pluton, South East Aswan, Egypt. Unpublished M.Sc. Thesis, Mansoura University, Mansoura.
- [10] Abdalla, H.M., Matsueda, H., Ishihara, S. and Miura, H. (1994) Mineral Chemistry of Albite-Enriched Granitoids at Um Ara, Southeastern Desert, Egypt. *International Geology Review*, **36**, 1067-1077. <http://dx.doi.org/10.1080/00206819409465505>
- [11] Roz, M.E. (1994) Geology and Uranium Mineralization of Gabal Gattar Area, North Eastern Desert, Egypt. Unpublished M.Sc. Thesis, Al Azhar University, Cairo, 175 p.
- [12] Abu Dief, A. (1985) Geology of Uranium Mineralization in Missikat, Qena-Safaga Road, Eastern Desert, Egypt. Unpublished M.Sc. Thesis, Assiut University, Assiut, 242 p.
- [13] Osmond, J.K., Dabous, A.A. and Dawood, Y.H. (1999) U Series Age and Origin of Two Secondary Uranium Deposits, Central Eastern Desert, Egypt. *Economic Geology*, **94**, 273-280. <http://dx.doi.org/10.2113/gsecongeo.94.2.273>
- [14] Abdel Naby, H.H. (2008) Genesis of Secondary Uranium Minerals Associated with Jasperoid Veins, El Erediya Area, Eastern Desert, Egypt. *Mineralium Deposita*, **43**, 933-944. <http://dx.doi.org/10.1007/s00126-007-0171-1>
- [15] NMA (Nuclear Material Authority) of Egypt (2003-2013) El Sela Development Project, Internal Reports.
- [16] Gaafar, I.M. (2005) Applications of Geological and Geophysical Survey for Defining the Uranium Potentiality of Some Younger Granites in the Eastern Desert of Egypt. Unpublished Ph.D., Faculty of Science, Mansoura University, Mansoura, 186 p.
- [17] Ali, K.G. (2011) Structural Control of El Sela Granites and Associated Uranium Deposits, South Eastern Desert, Egypt. *Arabian Journal of Geosciences*.
- [18] Abdel Gawad, A.E., Orabi, A.H. and Bayoumi, M.B. (2014) Uranium Evaluation and Its Recovery from Microgranite

- Dike at G. El Sela area, South Eastern Desert, Egypt. In Press.
- [19] Gaafar, I.M., Ghazala, H.H., Ibrahim, T.M. and Ammar, S.E. (2006) Gamma-Ray Spectrometry Studies for A Promising Vein Type Uranium Mineralization, South Eastern Desert, Egypt. *Proceedings of 4th International Symposium on Geophysics*, Tanta, 2006, 445-456.
- [20] Gaafar, I.M., Ghazala, H.H., Ibrahim, T.M. and Ammar, S.E. (2006) Application of Ground Magnetic Survey for Defining the Subsurface Structural Pattern of West Abu Ramad Shear Zone, Southern Eastern Desert, Egypt. *The 8th SEGJ International Symposium-Imaging and Interpretation*, Kyoto, 2006, 487-492.
- [21] Gaafar, I.M., Ghazala, H.H., Ibrahim, T.M. and Ammar, S.E. (2006) Conductivity Mapping Using VLF-EM Ground Survey For Promising Vein Type Uranium Mineralization, South Eastern Desert, Egypt. *8th International Conference of the Geology of the Arab World*, Cairo University, Giza.
- [22] Mayya, Y.S., Eappen, K.P. and Nambi, K.S. (1998) Methodology for Mixed Field Inhalation in Monazite Areas Using a Twin-Cup Dosimeter with Three-Track Detector. *Radiation Protection Dosimetry*, **77**, 177-184. <http://dx.doi.org/10.1093/oxfordjournals.rpd.a032308>
- [23] Debon, F. and Lefort, P. (1988) A Cationic Classification of Common Plutonic Rocks and Their Magmatic Associations: Principles, Method, Applications. *Bulletin de Mineralogie*, **111**, 493-510.
- [24] Sun, S.S. and McDonough, W.F. (1989) Chemical and Isotopic Systematics of Oceanic Basalts: Implications for Mantle Composition and Processes. In: Saunders, A.D. and Norry, M.J., Eds., *Magmatism in the Ocean Basins*, Vol. 42, Geological Society, Special Publications, London, 313-345.
- [25] Pearce, J.A., Harris, N.B.W. and Tindle, G. (1984) Trace Elements Discrimination Diagram for the Tectonic Interpretation of Granitic Rocks. *Journal of Petrology*, **25**, 956-983. <http://dx.doi.org/10.1093/petrology/25.4.956>
- [26] Saunders, A.D., Nory, M.J. and Tarney, J. (1991) Fluid Influence on the Trace Element Compositions of Subduction Zone Magmas. In: Tarney, J., Pickering, K., Knipe, R. and Dewey, J., Eds., *The Behaviour and Influence of Fluids in Subduction Zones*, Philosophical Transactions of the Royal Society of London, **335**, 377-392.
- [27] Nakamura, N. (1974) Determination of REE, Ba, Fe, Mg, Na and K in Carbonaceous and Ordinary Chondrites. *Geochimica et Cosmochimica Acta*, **38**, 757-775. [http://dx.doi.org/10.1016/0016-7037\(74\)90149-5](http://dx.doi.org/10.1016/0016-7037(74)90149-5)
- [28] Abd Elaal, H.A. (2006) Geochemistry and Processing of Some Valuable Metals from Mineralized Two Mica Granites, South Eastern Desert, Egypt. Unpublished M.Sc. Thesis, Cairo University, Giza, 110 p.
- [29] Speer, J.A., Solberg, T.N. and Becker, S.W. (1981) Petrography of the Uranium-Bearing Minerals of the Liberty Hill Pluton. South Carolina: Phase Assemblage and Migration of Uranium in Granitoid Rocks. *Economic Geology*, **76**, 2162-2175. <http://dx.doi.org/10.2113/gsecongeo.76.8.2162>
- [30] Wang, R., Cheng, F.F. and Monchoux, P. (1992) Minéraux disséminés comme indicateurs du caractère pegmatitique du granite de Beauvoir, massif d'Échassières, Allier, France. *Canadian Mineralogist*, **30**, 763-770.
- [31] Janeczek, J. and Ewing, R.C. (1992) Structural Formula of Uraninite. *Journal of Nuclear Materials*, **190**, 128-132. [http://dx.doi.org/10.1016/0022-3115\(92\)90082-V](http://dx.doi.org/10.1016/0022-3115(92)90082-V)
- [32] Miller, J.M. and Ostle, D. (1973) Radon Measurement in Uranium Prospecting. *Uranium Exploration Methods, Proceedings of a Panel*, Vienna, 10-14 April 1972.
- [33] Fleischer, R.L. and Mogro-Campero, A. (1978) Mapping of Integrated Radon Emanation for Detection of Long-Distance Migration of Gases within the Earth: Techniques and Principles. *Journal of Geophysical Research*, **83**, 3539-3549. <http://dx.doi.org/10.1029/JB083iB07p03539>
- [34] Weyer, S., Munker, C., Rehkemper, M. and Mezger, K. (2002) Determination of Ultra-Low Nb, Ta, Zr and Hf Concentrations and the Chondritic Zr/Hf and Nb/Ta Ratios by Isotope Dilution Analyses with Multiple Collector ICP-MS. *Chemical Geology*, **187**, 295-313. [http://dx.doi.org/10.1016/S0009-2541\(02\)00129-8](http://dx.doi.org/10.1016/S0009-2541(02)00129-8)
- [35] Linnen, R.L. and Cuney, M. (2008) Granite-Related Rare-Element Deposits and Experimental Constraints on Ta-Nb-W-Sn-Zr-Hf Mineralization. In: Linnen, R.L. and Samson, I.M., Eds., *Rare-Element Geochemistry and Mineral Deposits: Geological Association of Canada, GAC, Short Course Notes*, 17, 45-67.
- [36] Mann, A.W. and Deutscher, R.L. (1980) Solution Geochemistry of Lead and Zinc in Water Containing Carbonate, Sulfate and Chloride Ions. *Chemical Geology*, **29**, 293-311. [http://dx.doi.org/10.1016/0009-2541\(80\)90026-1](http://dx.doi.org/10.1016/0009-2541(80)90026-1)